STUDY OF THE EFFECTS OF OBSTACLES IN LIQUEFIED NATURAL GAS (LNG) VAPOR DISPERSION USING CFD MODELING

A Thesis

by

ROBERTO EDUARDO RUIZ VASQUEZ

Submitted to the Office of Graduate Studies of
Texas A&M University
in partial fulfillment of the requirements for the degree of

MASTER OF SCIENCE

August 2012

Major Subject: Safety Engineering

Study of the Effects of Obstacles in Liquefied Natural Gas (LNG) Vapor Dispersion using CFD Modeling

STUDY OF THE EFFECTS OF OBSTACLES IN LIQUEFIED NATURAL GAS (LNG) VAPOR DISPERSION USING CFD MODELING

A Thesis

by

ROBERTO EDUARDO RUIZ VASQUEZ

Submitted to the Office of Graduate Studies of
Texas A&M University
in partial fulfillment of the requirements for the degree of

MASTER OF SCIENCE

Approved by:

Chair of Committee,	M. Sam Mannan
Committee Members,	Charles J. Glover
	Cesar O. Malave
Head of Department,	Charles J. Glover

August 2012

Major Subject: Safety Engineering

ABSTRACT

Study of the Effects of Obstacles in Liquefied Natural Gas (LNG) Vapor Dispersion using CFD Modeling. (August 2012)

Roberto Eduardo Ruiz Vásquez, B.S., Pedro Ruiz Gallo University, Peru

Chair of Advisory Committee: Dr. M. Sam Mannan

The evaluation of the potential hazards related with the operation of an LNG terminal includes possible release scenarios with the consequent flammable vapor dispersion within the facility; therefore, it is important to know the behavior of this phenomenon through the application of advanced simulation tools. Computational Fluid Dynamic (CFD) tools are often used to estimate the exclusion zones in an event of accidental LNG spill. In practice these releases are more likely to occur in the confines of complex geometries with solid obstacles such as LNG terminals, and LNG processing plants.

The objective of this research is to study the effects that different obstacles have over the LNG vapor dispersion and the safety distance reduction caused by enhanced mixing. Through parametric analysis it is demonstrated that height, width and shape of the obstacles play an important role in the vapor concentration reduction. The findings of this research may be applied in the design stage of an LNG terminal, to improve the design of passive barriers, and for designing better layout configurations for storage

tanks. Simulations results performed with FLACS (Flame Acceleration Simulator), a CFD solver, confirmed that these applications help to reduce safety distances.

DEDICATION

To my parents Mario and Lila, for their motivation and advices during all this time, I will always be proud of being their son.

To my brother and sisters, Mario, Karla and Cecilia, who always believed in me.

To Isabel an especial person in my life, who is my partner and support in difficult times.

ACKNOWLEDGEMENTS

I would like to express my sincere gratitude to my advisor Dr. Sam Mannan, for his support and guidance throughout the course of my graduate studies and for giving me the opportunity to work on such an interesting topic.

I also would like to acknowledge to Dr. Subramanya Nayak for his excellent guidance and knowledge in computational fluid dynamics.

I would like to thank to Dr. Charles Glover and Dr. César Malavé, for serving as members of my advisory committee, for their time and suggestions in the development of this research.

Thanks also go to Towanna Arnold, Donna Startz and Valerie Green for making the paperwork easier during my time at Texas A&M University.

Finally, thanks to my family for their encouragement and love during all this process.

NOMENCLATURE

LNG	Liquefied Natural Gas
CFD	Computational Fluid Dynamics
FLACS	Flame Acceleration Simulator
t	Time
T	Temperature
LFL	Lower Flammability Limit
UFL	Upper Flammability Limit
MKOPSC	Mary Kay O'Connor Process Safety Center
NFPA	National Fire Protection Association

TABLE OF CONTENTS

Page

ABSTRACT iii

DEDICATION v

ACKNOWLEDGEMENTS vi

NOMENCLATURE vii

TABLE OF CONTENTS viii

LIST OF FIGURES xi

LIST OF TABLES xiv

CHAPTER

I BACKGROUND ON LNG 1

1.1 LNG definition 1
1.2 LNG safety hazards 2
1.2.1 Cryogenic hazards 2
1.2.2 Vapor-cloud fire 3
1.2.3 Pool fire 4
1.2.4 Torch fire 5
1.2.5 Rapid phase transition 6
1.2.6 Confined space explosion 6
1.3 Standards and regulations 6
1.3.1 DOT 49 CFR 193 6
1.3.2 NFPA 59A 7
1.3.3 U.S. Coast guard (USCG) regulations 7
1.4 Consequence analysis requirements 7
1.4.1 Estimation of the vapor cloud fire exclusion zone 8
1.4.2 Estimation of the pool fire thermal exclusion zone 8
1.5 Dispersion modeling and models classification 9
1.5.1 Dispersion modeling 9
1.5.2 Dispersion models classification 11
1.5.2.1 Workbooks/correlation models 12
1.5.2.2 Shallow layer models 12

CHAPTER Page

1.5.2.3 Integral models 12
1.5.2.4 CFD models 13
1.6 LNG experiments 14
1.6.1 Large scale experiments: Falcon tests 14
1.6.2 Medium and small scale experiments 16
1.6.2.1 BA-Hamburg trials 16
1.6.2.2 MKOPSC experiments 16
1.6.2.3 Other wind tunnel experiments 19

II INTRODUCTION 21

2.1 Motivation 21
2.2 Objectives 21
2.3 Methodology 22
2.4 Relationship with previous research in MKOPSC 24

III FLACS CAPABILITIES AND VALIDATION 27

3.1 Capabilities of FLACS in dispersion modeling 28
3.2 Mathematical models used in FLACS 28
3.2.1 Dispersion model 29
3.2.2 LNG pool model 33
3.3 Validation of FLACS against Falcon 1 test 39
3.3.1 Computational geometry and meshing 39
3.3.2 Simulation set up 41
3.3.3 Simulation results 42

IV PARAMETRIC ANALYSIS AND SIMULATION 45

4.1 Simulation set up 45
4.2 Vapor cloud behavior on different parameters 47
4.2.1 Shape effect 47
4.2.2 Height effect 49
4.2.3 Width effect 51
4.2.4 Roughness effect 53
4.2.5 Wind velocity effect 55
4.3 Parametric analysis 57
4.3.1 Analysis of pool release case 60
4.3.2 Analysis of jet release case 66

V POTENTIAL APPLICATIONS 72

CHAPTER Page

5.1 Analysis of aspect ratio and porosity 72
5.2 Special applications 78
5.2.1 Storage tanks' layout 78
5.2.2 Dike design 81

VI CONCLUSIONS AND FUTURE WORK 86

6.1 Conclusions 86
6.2 Future work 88

REFERENCES 89

VITA 94

LIST OF FIGURES

		Page
Fig. 1.1	Vapor cloud fire in China lake	4
Fig. 1.2	LNG pool fire	5
Fig. 1.3	LNG vapor dispersion phenomena	11
Fig. 1.4	Falcon 1 test configuration	15
Fig. 1.5	Position of measurement instrumentation in MKOPSC 2008 experiments (Data report of MKOPSC LNG spill tests: 2005-2009)	18
Fig. 1.6	Pit with wooden vapor fences used in MKOPSC experiments (Data report of MKOPSC LNG spill tests: 2005-2009)	18
Fig. 1.7	Flow around a cube normal to the flow in a wind tunnel	19
Fig. 1.8	Flow around a cylinder normal to the flow in a wind tunnel.	20
Fig. 2.1	Research methodology	24
Fig. 2.2	Relationship of this research with previous work in LNG vapor dispersion at MKOPSC	26
Fig. 3.1	Computational geometry generated in FLACS for Falcon1 test	40
Fig. 3.2	Detail of meshing and refinement on the simulation domain.	41
Fig. 3.3	FLACS validation against experimental data and FLUENT simulation	44
Fig. 4.1	Location of the source and measurement points for gas concentration in the cases of: cube (a) and cylinder (b)	46
Fig. 4.2	Shape effect on vapor cloud for cube (a) and cylinder (b).	48
Fig. 4.3	Concentration values along the centerline for cube and cylinder	49

Page

Fig. 4.4 Height effect on vapor cloud for a 3m cube (a) and increased height of cube to 6m (b) 50

Fig. 4.5 Concentration values and reduction efficiency for cube and cylinder... 51

Fig. 4.6 Width effect on vapor cloud for a 3m cube (a) and increased width of cube to 6m (b) 52

Fig. 4.7 Concentration values and concentration reduction for cube and cylinder with increased width 53

Fig. 4.8 Cloud shape for the cube with roughness 0.0002 (a) and 0.03 (b) 54

Fig. 4.9 Concentration values and concentration reduction for cube and cylinder with different roughness values 55

Fig. 4.10 Wind velocity effect for a velocity of 1.5 m/s (a) and 6 m/s (b) 56

Fig. 4.11(a) Pareto chart with effects and significance of parameters at downwind distance: x = 3m. 61

Fig. 4.11(b) Pareto chart with effects and significance of parameters at downwind distance: x = 82.5m 62

Fig. 4.12 Surface plots of parameter interaction at distance: x = 3m..... 64

Fig. 4.13 Surface plots of parameter interaction at distance x = 82.5m 65

Fig. 4.14(a) Pareto chart with effects and significance of parameters at downwind distance: x = 3m 66

Fig. 4.14(b) Pareto chart with effects and significance of parameters at downwind distance: x = 82.5m 67

Fig. 4.15 Surface plots for parameter interaction at distance: x = 3m 70

Fig. 4.16 Surface plots for parameter interaction at distance: x = 82.5m 71

Fig. 5.1 Linear tank's arrangement for aspect ratio and porosity analysis 73

Fig. 5.2 Flammability contours through tanks with three different aspect ratios: (a) 1, (b) 1.5, and (c) 2 75

Page

Fig. 5.3 Concentration reductions at different aspect ratios and porosities at 50m from the storage area border line 76

Fig. 5.4 Flammability contours through tanks with three different aspect ratios (staggered layout) 79

Fig. 5.5 Comparison of flammability contours at different tank's layout, with aspect ratio =2, at t = 750 s 80

Fig. 5.6 Comparison between two different dike designs, dike 1: 110 x 110 x 5 m, dike 2: 85 x 85 x 8 m 82

Fig. 5.7 Pool formation within dike 2 at time 600 seconds..... 83

Fig. 5.8 Comparison between safety distances with the two different analyzed dikes 84

Fig. 5.9 Safety distance reduction with two different dike dimensions 85

LIST OF TABLES

		Page
Table 1.1	Physical properties of methane	2
Table 3.1	Relationship between Monin-Obukhov length and atmospheric stability	30
Table 3.2	Wind profile parameters: Ls, Zs, and h (adapted from Bosch & Weterings, 2005; Golder, 1972; and Han et al., 2000).	31
Table 4.1	Simulation details for parametric analysis in pool release case	58
Table 4.2	Simulation details for parametric analysis in jet release case.	59
Table 4.3	Parameter values for pool and jet releases.	60
Table 4.4	Parameter contribution in the concentration reduction for pool release case at distances: x = 3 m and x = 82.5 m	63
Table 4.5	Parameter contribution in concentration reduction for jet release case at distances: x = 3 m and x = 82.5 m	68
Table 5.1	Concentration reduction percentage at different tanks' layout	81

CHAPTER I

BACKGROUND ON LNG

1.1 LNG DEFINITION

Liquefied Natural Gas (LNG) is an odorless, clear cryogenic liquid produced by cooling natural gas to about 111 Kelvin (K). In its liquid state, the volume of LNG is about 600 times less than its gaseous state. This reduction in volume allows economical long distance transportation of LNG by ships to LNG terminals. In these terminals, LNG is reconverted to its gaseous state to be used in houses, industries, and power plants (EIA, 2009).

The LNG composition is mainly 95% methane; however, it also contains ethane, propane and other heavier hydrocarbons. An important property of cold LNG vapor is that it is heavier than air by a factor of 1.5; therefore, LNG spills results initially into heavy gas clouds. Table 1.1 shows the main physical properties of methane.

This thesis follows the style of the *Journal of Loss Prevention in the Process Industries*.

Table 1.1 Physical properties of methane (adapted from white paper: LNG pool fire modeling-MKOPSC, 2008):

Property	Value	Units
Molecular Weight	16.04	kmol/kg
Freezing point	90.00	K
Boiling point (B.P)	111.70	K
Liquid density at B.P	450.00	kg/m^3
Critical temperature	190.60	K
Critical pressure	4.64E+06	Pa

1.2 LNG SAFETY HAZARDS

Following potential hazards are identified in the case of an LNG release in a facility: cryogenic hazards, vapor c8loud fire, pool fire, torch fire, rapid phase transition, and confined space explosion (MKOPSC, 2008).

These hazards are explained in detail in the paragraphs that follow.

1.2.1 Cryogenic hazards

This type of hazard is created because LNG has to be stored and transported at very low temperatures, around 111 K. At these below freezing temperatures there are negative effects on a living tissue.

Also, the containment and structural materials containing the LNG can be damaged and fail by embrittlement. Therefore, special attention is needed in selecting adequate materials to withstand cryogenic temperatures. For instance, structures with 5-9% of nickel steel are required in LNG tanks and other process components in contact with the LNG (Cormier et al., 2009).

1.2.2 Vapor-cloud fire

In the case of a release, a vapor cloud is generated by the LNG boiling and mixing with the surrounding air. When the cloud is first dispersed it is heavier than air, then it is further mixed and diluted with more air as it goes downwind. Flammable limits of the LNG cloud range from 5 to 15% in volume concentration, and it becomes hazardous when during its traveling path an ignition source is found. If this flammable cloud ignites, the resulting flame will propagate through the cloud and then back to the source. Figure 1.1 shows an example of vapor cloud fire from the China Lake experiments. Vapor cloud fire can cause severe burns to people in its influence zone, and also it could damage equipment depending on the exposure time (Raj, 2007).

Fig 1.1. Vapor cloud fire in China lake (Raj, 2007)

1.2.3 Pool fire

LNG releases of sufficient flow rate and time could create a pool on the ground. In the case of ignition it will create a pool fire. As can be seen in figure 1.2, the effects of a pool fire are localized but it has a longer duration in comparison with a vapor cloud fire; therefore, it is possible that the pool fire will remain and expand if a spill continues feeding the pool (Qiao et al., 2006).

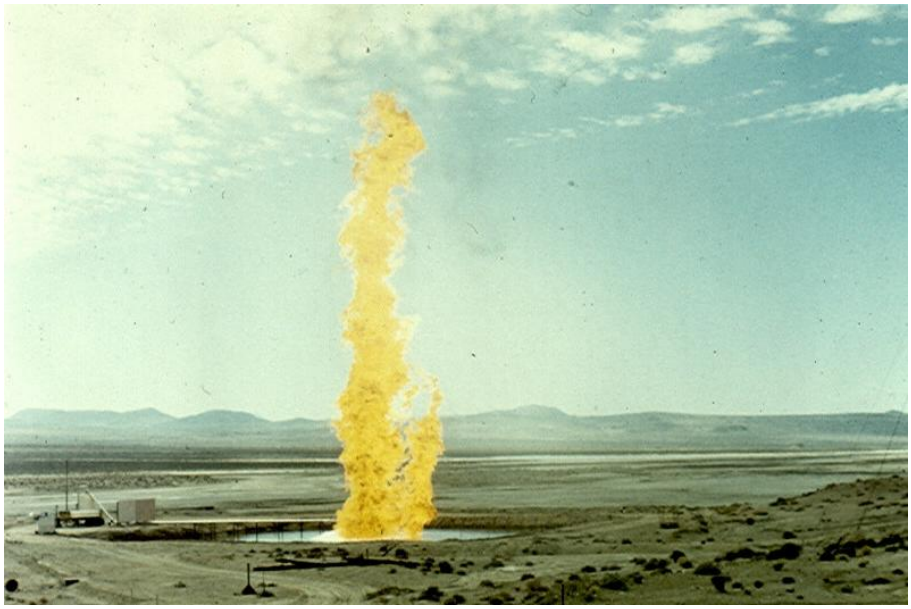

Fig. 1.2. LNG pool fire (Raj, 2005)

1.2.4 Torch fire

When a release comes from pressurized containment, a spray with liquid droplets is formed. In the case of ignition, a torch fire is developed leading to direct flame with radiant heating. In comparison with pool fires, torch fires present the same type of hazard, but a torch fire is often greater than a pool fire; because the torch fire tends to produce a larger flame.

1.2.5 Rapid phase transition

This phenomenon has been observed in the case of LNG release on or under water, with a characteristic spontaneous generation of vapor as the cold LNG is vaporized from heat gained from the spill surface, and with a flameless explosion.
The hazard potential of rapid phase transitions can be severe; however, they will not propagate further than in the immediate vicinity of the spill area (Qiao et al., 2006).

1.2.6 Confined space explosion

This type of hazard occurs when the vapor cloud traveling downwind finds a confined space, where in the case of ignition the accumulated vapor could lead to an explosion. The damage caused by this explosion could be small or large depending on whether the pressure limit of a building is exceeded.

1.3 STANDARDS AND REGULATIONS

1.3.1 DOT 49 CFR 193

This U.S. Federal standard was promulgated by the Department of Transportation (DOT) under the title: 49 CFR 193, “Liquefied Natural Gas Facilities: Federal Safety Standards”. This regulation covers siting requirements, design and construction, equipment, operations, maintenance, fire protection, and security.

Regarding the safety requirements in an LNG facility, an impounding system is necessary as well as calculations of vapor dispersion and thermal exclusion zones to ensure public safety beyond a given facility’s fence line.

1.3.2 NFPA 59A

The National Fire Protection Association (NFPA) covers information related to safety and security in process systems, storage areas, piping systems handling LNG through the NFPA 59A: "Standard for the Production, Storage, and Handling of Liquefied Natural Gas (LNG)". Impounding systems that can contain a possible LNG spill, as well as dispersion and thermal exclusion zones, also are required under NFPA 59A. Exclusion zones extend from the point of the release to the distance reached by the vapor cloud in terms of the half Lower Flammability Limit (LFL).

1.3.3 U.S. Coast guard (USCG) regulations

This regulation entitled as "Liquid Flammable Gases," is related to tanker design and facility sitting. It determines how to transport LNG safely and requires the use of manuals where ships operate. Safety rules also are required for specific ports to reduce accident risk.

1.4 CONSEQUENCE ANALYSIS REQUIREMENTS

Vapor cloud fires and pool fires are two main hazards in an LNG facility, which have a delayed and immediate potential of ignition, respectively. Regulations such as NFPA 59A and 49 CFR 193 provide procedures to analyze the consequences of these hazards in an LNG facility, allowing the design engineer to apply creative solutions to mitigate catastrophic events.

1.4.1 Estimation of the vapor cloud fire exclusion zone

Regulations such as 49 CFR 193 require the estimation of pool fire and vapor cloud safety distances through simulation tools (U.S. Department of Transportation, 2002). This regulation allows using software such as DEGADIS and FEM3A to perform vapor dispersion simulations; while for pool fire simulations the allowed software is LNGFIRE3.

NFPA 59A defines "accidental design spill" as the most representative and likely-to-occur spill; based on historical experience and special features in an LNG facility. Design spills must be used as inputs in consequence analysis of an LNG facility and its surrounding area.

The spill volume is calculated using the following equation:

$$\text{Spill Volume} = [(\text{Spill Time}) \times (\text{Flow Rate})] + \text{Pipe Drainage} \quad (1.1)$$

Definition of a design spill is basically the same in 49 CFR 193 regulation, with exception of the process transfer area. The use of a continuous release is present in both NFPA 59A and 49 CFR 193 standards.

1.4.2 Estimation of the pool fire thermal exclusion zone

In the event of a pool fire, people and property could be severely affected by the radiation and contact with flames; therefore, determination of fire thermal exclusion zone is necessary and required by U.S regulations. The estimation of this exclusion zone

has different approaches depending on the assumed scenario involved, although the equations to calculate them are similar.

Requirements for modeling hazard scenarios are given by 49 CFR 193 and NFPA 59A (section 2) regulations, and they are focused on large volume LNG storage areas. LNGFIRE simulation model is required by NFPA to calculate thermal radiation distances, and its predictions are based on calculation of basic flame geometry and surface radiation flux. Other alternative models are available, and they have been validated by experimental data taking into account the same physical factors.

Regulations such as the European EN 1473:1997 describe maximum thermal radiation flux at the property boundary in an LNG facility, with values of 5 kW/m^2 for urban areas, and 1.5 kW/m^2 for critical areas.

1.5 DISPERSION MODELING AND MODELS CLASIFICATION

1.5.1 Dispersion modeling

The modeling of the vapor dispersion phenomena is mainly due to two main steps: the source term and vapor dispersion. For this research the source term is modeled by a pool formation from an LNG spill; on the other hand, the vapor dispersion describes the physical process of the gas entrainment in the air and its posterior dilution.

Figure 1.3 describes the phenomena involved in vapor dispersion. The source term represents the evaporation rate for a given release scenario. The most common scenario is the pool formation due to a continuous LNG release in a confined area. The evaporation rate depends mainly on the heat transfer between the liquid pool and the

contacted surface. In the case of a release on ground, the evaporation rate will decrease over time, because the freezing effect of the ground in contact with the cold LNG. If the pool is formed on water, the evaporation rate will be more continuous, and it will depend on the turbulence created during the release (Cormier, 2008).

Once the source term is initiated, the phenomenon of vapor dispersion downwind follows. In the case of LNG, the dispersion follows a heavier-than-air gas behavior, because its density and cold temperature.

At the beginning, the evaporation is caused by the heat transfer from the surroundings, with a quick vapor expansion and negative buoyancy effects. Then, the wind entrainment creates a horizontal mixing and dilution of the vapor. In this stage, the vapor has a neutral buoyancy but as it travels downstream it becomes positive buoyant. Atmospheric conditions also play an important role; for instance, during unstable atmospheric conditions the buoyancy turbulence is present, while during stable conditions the turbulence is negligible (Cormier, 2008).

Figure 1.3 also indicates the flammable region of LNG, which ranges from 5% (Lower Flammability Limit, LFL) to 15% (Upper Flammability Limit, UFL). The concept of exclusion zone or safety distance is defined as the point when the LNG gas mixture is below the Lower Flammability Limit (LFL); therefore, after that distance the vapor cloud will not ignite.

The purpose of this section was to explain briefly the phenomena involved in the dispersion modeling; the equations for pool formation and vapor dispersion are explained in detail in Chapter III.

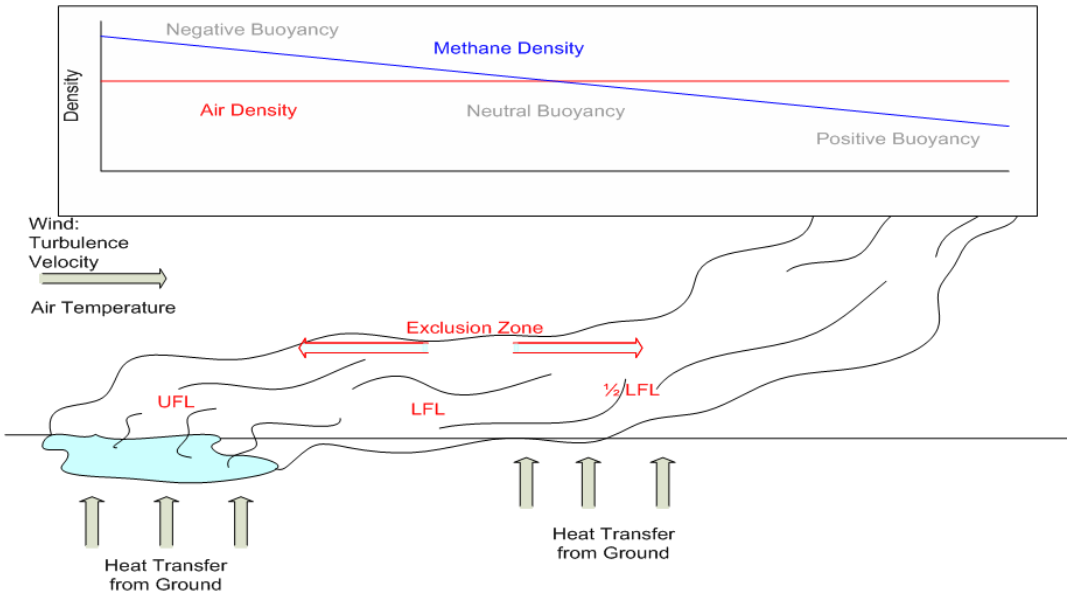

Fig. 1.3. LNG vapor dispersion phenomena (Cormier, 2008)

1.5.2 Dispersion models classification

A wide range of models for LNG vapor dispersion is available to assess the scenario of an LNG spill. For a better understanding of the capabilities and limitations of these models, they can be categorized in four groups: Workbooks/correlations, Shallow layer models, Integral models, and Computational Fluid Dynamics (CFD) models.

1.5.2.1 Workbooks/correlation models

This type of model uses empirical relations to solve two given quantities. The model expresses the spreading rate in terms of correlations between downstream distance and atmospheric stability. The main advantages of this model are its simplicity and quick application; however, it can only be applied to simple scenarios because it presents limitations in complex situations (Crowl & Louvar, 2002).

1.5.2.2 Shallow layer models

They have a combination of some features of integral and CFD models. For a dense gas simulation, depth-averaged variables are used to predict the flow behavior. This model is physically realistic and ideal to simulate dispersion over sloping terrain, because they are less empirical than integral models but easier to use than CFD models. However, they need more computational time in comparison with integral models; for that reason, they are not broadly used in commercial applications and are more popular for research purposes (Hankin, 2003).

1.5.2.3 Integral models

Differential equations are used in these models to describe the integral properties of a flow. In the case of heavy gas clouds, this model uses a cylindrical box considering radius and volume properties varying over time. For this reason, this model is also known as a box model.

Source and dispersion are commonly used separately in integral models; for the case of LNG, the source is often modeled as a pool. For the case of dispersion, this model allows different properties such as wind speed, surface roughness and atmospheric stability, but these properties are modeled as constant over time (Spicer & Havens, 1987).

Some advantages of using this model are its good prediction capability and its quick run on the simulated scenarios. For this reason, they are broadly used for hazard assessments. The main disadvantage of these models is that they usually do not take into account obstacles or non-flat terrain in the calculation; therefore, sometimes the results obtained with these models are conservative. Some examples of common integral models include SLAB, DEGADIS, and PHAST (Puttock, 1987).

1.5.2.4 CFD models

This type of model develops a numerical solution using Navier-Stokes equations for three dimensional time-dependent flow equations. Its main advantage is the inclusion of the effects of complex geometries, such tanks or dikes, in the simulation solution on flow and dispersion. The approach in simulating vapor dispersion is more realistic and accurate than other models (Chan, 1992). The main disadvantage of this model is the required simulation time, which can be a few hours or many days, depending on the complexity of the scenario and computational meshing involved. Another disadvantage is the relative difficulty during the set up process and the significant computer resources

needed; for this reason, this type of simulation must be performed by an experienced user (Chan, 1994).

Some examples of CFD models widely used are FEM3A, FLUENT, CFX, and FLACS. Most of them have been validated against full scale or wind tunnels experiments.

1.6 LNG EXPERIMENTS

1.6.1 Large scale experiments: Falcon tests

The most significant field trial experiments of LNG release in the presence of obstructions are the Falcon trials undertaken in 1987. The Falcon tests were large scale experiments developed in 1987 by Lawrence Livermore National Laboratories at Frenchman Flat, Nevada. The intention of the tests were to evaluate the effectiveness of vapor barriers on mitigating the hazard distance produced in an eventual LNG release and also to provide broad data for future validation studies (Brown et al., 1990).

Five LNG spills were created with volumes from 20 m^3 to 63 m^3 onto a water pond equipped with a water circulation system to stimulate rapid vaporization of the LNG and to assure that the evaporation rate was as close as possible to the spill rate.
An uniform LNG distribution on the pond was provided by a spill “spider” system, which consisted of a main pipe with 4 smaller pipes in its extreme; each small pipe had 0.11 m in diameter and was spaced 90 degrees between each other.

A vapor fence was constructed around the water pond using fiberglass material, with dimensions of 44 m by 88 m and a height of 8.7 m. A billboard structure with

dimensions of 17.1 m wide and 13.3 m height, was located upwind the water pond in order to simulate the turbulence effect of a storage tank inside the fence. The experimental setup of the Falcon 1 test is shown in Figure 1.4.

Temperature and gas concentration values along the path of the vapor cloud were of special interest in this experiment. An array of sensors for these parameters were located in stations at 50 m, 150 m, and 250 m downwind the water pond; at heights of 1 m, 5 m, 11 m and 17 m above to the ground.

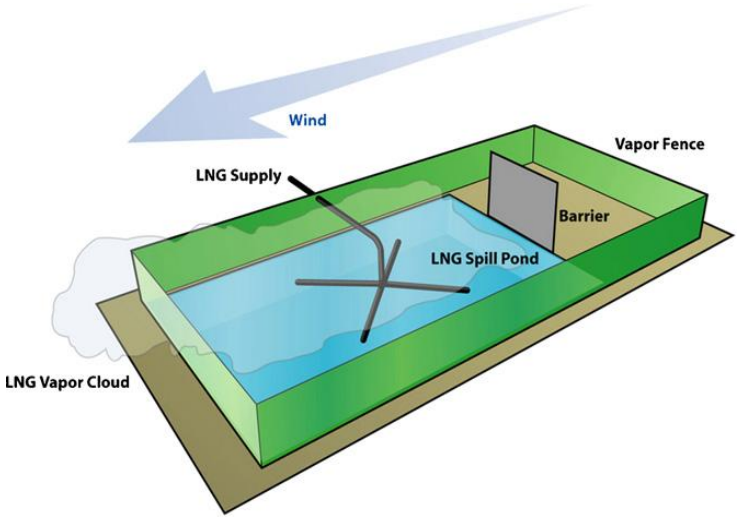

Fig. 1.4. Falcon 1 test configuration (Gavelli et al., 2008)

1.6.2 Medium and small scale experiments

In previous years, a series of medium and small scale experiments have been performed to analyze the behavior of vapor dispersion including the presence of obstacles. Some of the most relevant experiments carried out are explained below.

1.6.2.1 BA-Hamburg trials

These experiments were carried out by the Meteorological Institute at the University of Hamburg. Open wind tunnel was used to study several configurations during the BA-Hamburg trials, under scenarios of instantaneous and continuous releases.

Some of these configurations include crosswind canyons, sloping terrain, semicircular fence placed upwind or downwind from a release, and a fence completely surrounding a release (Coldrick et al., 2010). The fences were located downwind from the release, perpendicular or in angle with the wind direction.

These experiments provided of useful data on dense gas dispersion for further studies and validation purposes.

1.6.2.2 MKOPSC experiments

From the years 2005 to 2009, six series of small and medium scale experiments were performed by MKOPSC and TEEX, at the Brayton Fire Training Field (BFTF). During the development of these experiments, LNG containing 98-99.8% methane was spilled inside three different concrete pits. The pits contained water inside them, with the purpose to promote a constant amount of LNG vaporization, equal to the LNG discharge

rate. In order to reduce the vertical fluid momentum at the moment of the discharge, a metal plate was located under the pipe discharge end.

Weather conditions were measured before and during the tests; for instance humidity, wind direction and velocity, atmospheric temperature and pressure. Also, other parameters of interest for vapor dispersion, such as gas concentration and temperature were also measured at different locations and heights along the path of the vapor cloud. Figure 1.5 shows the position of the poles with the measurement instrumentation over the predicted path of the vapor cloud, using the setup for the experiments of the year 2008 (MKOPSC, 2010).

In the experiments performed from the years 2007 to 2009, wooden boards with a height of 6 feet were located around the pits. The reason was to simulate the effect of vapor fences in retaining the LNG vapor inside the pits. The experiment results demonstrated that vapor fences hold up the vapor cloud increasing the turbulence effects inside the pit and for that reason, they help to reduce significantly the safety distance downwind.

Figure 1.6 illustrates the pit with wooden vapor fences around it. Also, poles with measurement instruments and the metal plate under the discharge pipe are showed.

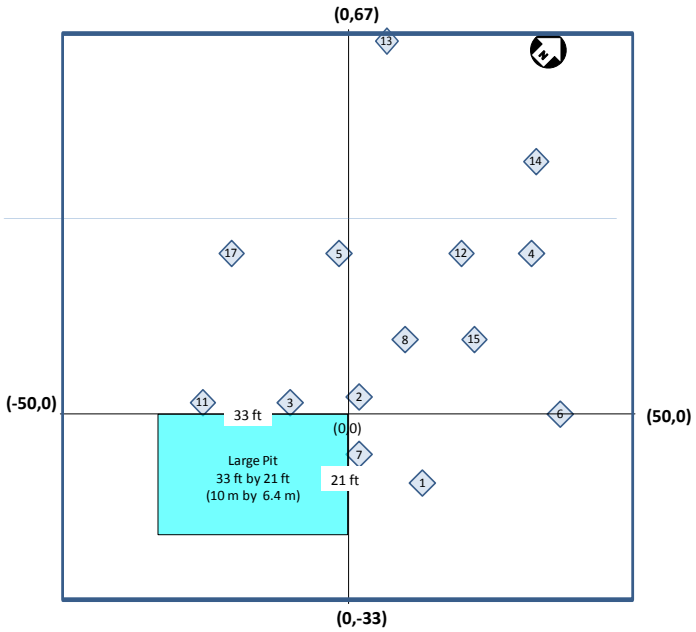

Fig. 1.5. Position of measurement instrumentation in MKOPSC 2008 experiments (Data report of MKOPSC LNG spill tests: 2005-2009).

Fig. 1.6. Pit with wooden vapor fences used in MKOPSC experiments (Data report of MKOPSC LNG spill tests: 2005-2009).

1.6.2.3 Other wind tunnel experiments

Previous wind tunnel and full scale experiments were developed in order to evaluate the effects that simple geometries, such as cube and cylinder, have over the vapor dispersion. Robins and Castro first addressed this topic in 1977, through wind tunnel experiments analyzing the process involved in plume dispersion in the vicinity of a cube, finding flow patterns and concentration values downwind (Robins & Castro, 1977). Further experiments were developed in 1993 (Martinuzzi & Tropea, 1993) and in 2003 (Mavroidis et al., 2003).

With regard to the full scale experiments, Ogawa and Oikawa developed field studies in 1982, intended to study the cavity wake behind a cube with different wind directions (Ogawa & Oikawa, 1982). Also Macdonald studied the effects of an array of these geometries in 1998 (Macdonald et al, 1982). Figures 1.7 and 1.8 show the flow around cube and cylinder geometries in wind tunnel experiments (Mavroidis et al., 2003).

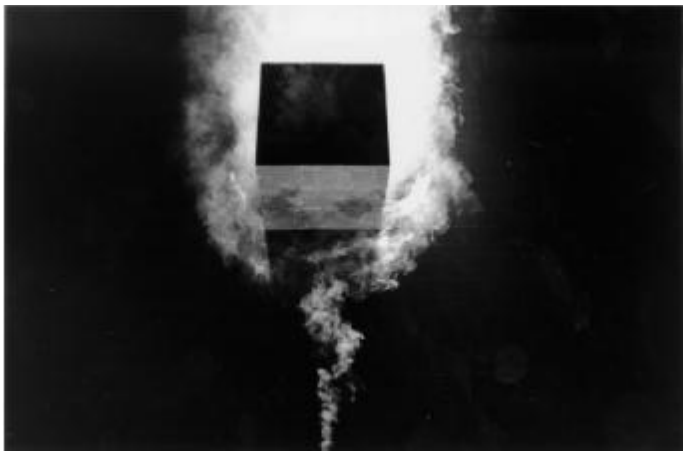

Fig 1.7. Flow around a cube normal to the flow in a wind tunnel (Mavroidis et al., 2003)

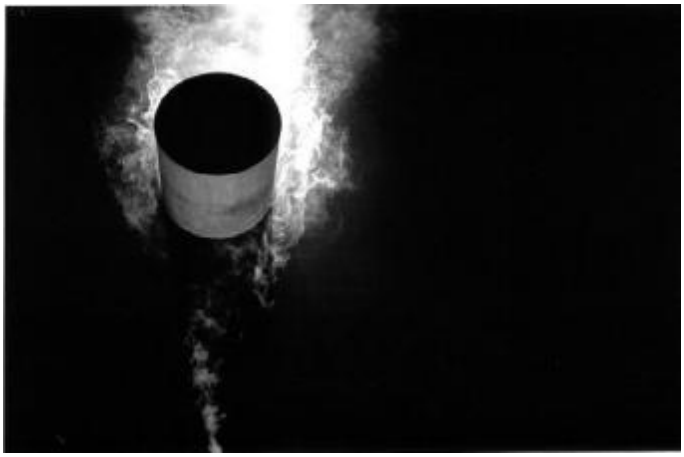

Fig 1.8. Flow around a cylinder normal to the flow in a wind tunnel (Mavroidis et al., 2003)

CHAPTER II

INTRODUCTION

2.1 MOTIVATION

The design of an LNG (Liquefied Natural Gas) terminal and facility requires the evaluation of the potential hazards related with its operation, which includes possible release of LNG, resulting in flammable vapor dispersing within the facility (NFPA, 2009). Safety distances are required to prevent damage outside the facilities in the case of an LNG release, and regulations such as 49 CFR 193 and standard NFPA 59A require the application of advanced simulation tools to assess safety distances for accidental release scenarios.

Several studies in vapor dispersion have been performed in the past; however, there are few studies about the effects of passive barriers in reducing the safety distance by using CFD (Computational Fluid Dynamic) models. This research has the purpose to fill this gap.

2.2 OBJECTIVES

The main goal of this research is to acquire a better understanding about the effects that different geometries (obstacles) may have over LNG vapor dispersion, and how much the safety distance could be reduced in presence of these obstacles. To accomplish these objectives, commercial CFD software FLACS (Flame Acceleration

Simulator) is used; given its ability to accurately simulate the dispersion of an LNG vapor cloud (Hansen et al., 2010).

The main objectives of this research include:

- To develop a CFD model tool that can be used for simulating LNG vapor dispersion through obstacles.
- Validation of developed model against a large scale experiment (Falcon 1 test).
- To perform a parametric analysis over the main parameters involved in vapor dispersion to determine their significance in vapor concentration reduction.
- To develop a methodology to assess the vapor concentration reduction through the study of tank aspect ratios and porosities within an LNG storage area.
- Application of a CFD model to assess two specific cases: a better design for dikes, as well as a better layout configuration for storage tanks in an LNG facility. The goal of both applications was to obtain a reduction in the vapor concentration, reducing the safety distance.

2.3 METHODOLOGY

The method used in this research includes the validation of the Flame Acceleration Simulator (FLACS) in accurately simulating LNG vapor dispersion. For validation purposes, large scale experimental data from the Falcon tests, and small scale experimental data from the MKOPSC tests are used. Large scale experiments considered spill volumes of about 40 m^3 per release while small scale that amount was about 5 m^3.

The next step is to study the effects of the obstacles in vapor dispersion. The main geometries found in an LNG facility (for instance, in an LNG terminal) are tanks and buildings. In this analysis they will be represented as solid cylinders and cubes; the exact details of these geometries will be not considered. In future, the methodology developed in this study can be easily applied to a specific detailed geometry. Concentration measurement points were considered downwind of the studied obstacles to gather vapor concentration values.

In order to know which parameters play a more important role in the vapor concentration reduction, a parametric analysis will be done. The knowledge gained from this analysis will then be applied to determine optimal passive barriers and LNG tank farm layout. Figure 2.1 shows the steps that are used to achieve the research objectives.

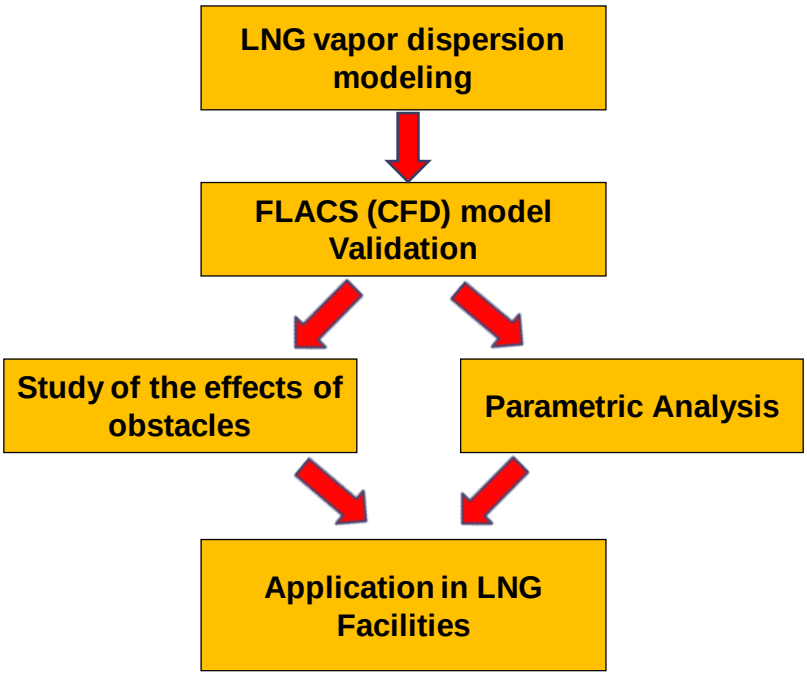

Fig. 2.1. Research methodology

2.4 RELATIONSHIP WITH PREVIOUS RESEARCH IN MKOPSC

This research will expand the knowledge reached so far by the MKOPSC in studying and simulating LNG vapor dispersion scenarios. Figure 2.2 shows the findings of the MKOPSC about this topic and its relationship with this research. In 2008, Ben Cormier conducted a study of the key parameters for vapor dispersion modeling using CFX code to determine their effect on LNG vapor dispersion. Also, he analyzed the concentration and temperature values of vapor clouds and performed a sensitivity analysis over the source term and atmospheric effects (Cormier, 2008).

In 2011, Ruifeng Qi performed a source term study on LNG underwater release. His research focused on the measurement of the reduction in the safety distance with the use of vapor fences around a pit, comparing a scenario with-fence versus with-no-fence. Validation of the experimental data of the MKOPSC using the CFX code was performed, along with a sensitivity analysis for the mesh size and the source term turbulence (Qi, 2011).

As mentioned earlier, this research will use the previous findings in order to analyze the effects of passive barriers in vapor dispersion using CFD code by modifying the shape, height, and width of passive barriers and also the roughness and wind speed. Parametric analysis will be used to quantify the effects of obstacles and passive barriers in vapor dispersion phenomena.

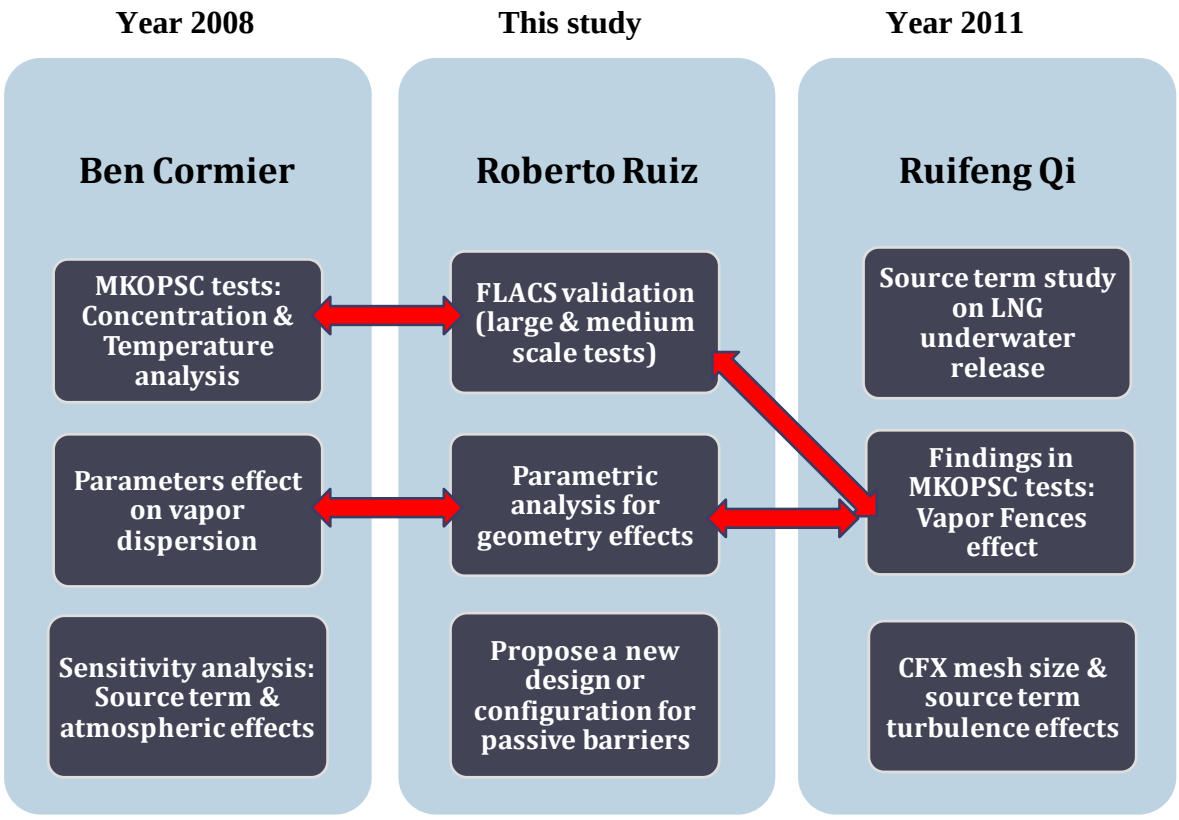

Fig 2.2. Relationship of this research with previous work in LNG vapor dispersion at MKOPSC

CHAPTER III

FLACS CAPABILITIES AND VALIDATION

FLACS is a CFD tool that can address complex scenarios and it is commonly used for dispersion modeling of flammable and toxic gases. This tool was developed in 1980 at the Department of Science and Technology at Christian Michelsen Institute (CMI); some years later they established Gexcon as a consultant company which currently holds the property rights of the FLACS code (Gexcon AS, 2011).

Previous studies have been carried out reviewing many aspects of FLACS such as the studies performed in 2004 (Hanna et al., 2004) and in 2008 (Hansen et al., 2008). Also, independent studies by the Health and Safety Laboratory have been done. Lately, a validation of FLACS against gas dispersion experiments was performed following the Model Evaluation Protocol (Hansen et al., 2010).

On October 7, 2011, FLACS was approved to be used for modeling vapor dispersion scenarios by The Pipeline and Hazardous Materials Safety Administration (PHMSA) of the U.S. Department of Transportation. In this manner, FLACS is the only approved model for simulating LNG dispersion scenarios for facility siting in the United States (Gexcon website, 2012).

This chapter will explain the capabilities and mathematical models used by FLACS; for instance, the dispersion model which solves the Reynolds-averaged-Navier-Stokes (RANS) equations on a non-uniform Cartesian grid. In the case of the pool model, governing equations and the expressions for a spreading pool are presented.

3.1 CAPABILITIES OF FLACS IN DISPERSION MODELING

This software presents many advantages in simulating different scenarios such as dense or buoyant gases in open or obstructed environments. Documentation for validation of FLACS is available from different papers or from Gexcon website, and the results obtained are in good agreement with experimental data.

A feature that makes FLACS distinct from other CFD models is its distributed porosity model for small and sub-grid scale obstacles; which allows a relative rapid simulation in comparison with other CFD codes. In general purpose CFD codes the source model is not usually available; however, FLACS includes source models for evaporating pools as well as for flashing and high-pressure releases.

Set up options for different boundary conditions also are available in this software, which takes into account atmospheric stability classes and surface roughness in the simulation domain. Furthermore, FLACS includes a suitable turbulence model and solution methods such as wall functions, pressure correction algorithms and spatial discretization schemes.

3.2 MATHEMATICAL MODELS USED IN FLACS

LNG dispersion modeling involves two main steps: the pool source and its posterior vapor dispersion. This section will cover the mathematical equations used by FLACS to address both phenomena.

3.2.1 Dispersion model

FLACS approaches vapor dispersion by solving the Reynolds-averaged-Navier-Stokes (RANS) equations on a non-uniform Cartesian grid. The model allows including temperature profiles as a function of Pasquil-Gifford stability classes; and also wind velocity, turbulence, and surface roughness length (z_0) are considered.

Properties of the atmospheric boundary layer on the floor's surface are reproduced by using wind boundaries. The buoyancy effects on the atmospheric boundary layer are explained by the characteristic length scale, which is shown in the equation 3.1 (Monin & Obukhov, 1954).

$$L = -\frac{\rho_a \, c_p \, T_a \, u^{*3}}{\kappa \, g \, H_s} \qquad (3.1)$$

In equation, u* is the friction velocity and Hs is the sensible heat flux from the surface. Stability of the atmospheric boundary can be measured by the value of the Monin-Obukov length.

Table 3.1 shows the relationship between Monin-Obukov lengths and the atmospheric stability (Bosch & Weterings, 2005).

Table 3.1 Relationship between Monin-Obukhov length and atmospheric stability (adapted from Bosch & Weterings, 2005).

Monin-Obukhov length	**Stability Condition**
Small negative, -100m < L0	Very unstable
Large negative, $-10^5 < L < -100$	Unstable
Very large, $L > 10^5$	Neutral
Large positive, $10 < L < 10^5$	Stable
Small positive, $0 < L < 10$	Very stable

To estimate the Monin-Obukhov length, FLACS uses the Pasquill stability classes which indicate the level of turbulence present in the atmosphere. In the initial set up the user has to include the wind velocity (U_0) at a reference height (z_{ref}), the Pasquill stability class, and also the atmospheric roughness length (z_0).

The logarithmic velocity profile is given by equation 3.2.

$$U(z) = \begin{cases} \frac{u^*}{k} \ln\left(\frac{(z-z_d)+z_0}{z_0}\right) - \psi_u(z) & \text{if } z_0 > 0 \\ U_0 & \text{if } z_0 = 0 \end{cases} \tag{3.2}$$

$$u^* = \frac{U_0 \kappa}{\ln\left(\frac{(z_{ref}-z_d)+z_0}{z_0}\right) - \psi_u(Z_{ref})} \tag{3.3}$$

In the equation (3.3), u* is the friction velocity and z_d is the canopy height.

Term ψ_u is defined in the next equation:

$$\psi_u(z) = \begin{cases} 0 & \text{for Pasquill class D} \\ 2\ln\left(\frac{1+\xi}{2}\right) + ln\left(\frac{1+\xi^2}{2}\right) - 2\arctan(\xi) + \frac{\pi}{2} & for\ L < 0 \\ -17\left(1 - \exp\left(-0.29\frac{z}{L}\right)\right) & for\ L > 0 \end{cases} \quad (3.4)$$

where $\xi = (1 - 16\ z/L)^{1/4}$ (3.5)

Table 3.2 shows the wind profile parameters used to calculate velocity, k, and ε values at wind boundaries.

Table 3.2 Wind profile parameters: Ls, Zs, and h (adapted from Bosch & Weterings, 2005; Golder, 1972; and Han et al., 2000).

Pasquill class	Stability	Boundary layer height, h	Ls	Zs
A	Unstable	1500 m	33.162 m	1117 m
B	Unstable	1500 m	33.258 m	11.46 m
C	Slightly unstable	1000 m	51.787 m	1.324 m
D	Neutral	$0.3u^*\frac{L}{f}$	1.0 m	0 m
E	Slightly stable	$0.4\sqrt{\frac{u*L}{f}}$	- 48.33 m	1.262 m
F	Stable	$0.4\sqrt{\frac{u*L}{f}}$	- 31.323 m	19.36 m

A simpler way to calculate the Monin-Obukhov length is by Golder's equation which uses the values from Table 3.2 (Golder, 1972).

$$\frac{1}{L} = \frac{1}{L_s} \log \frac{z_0}{z_s} \tag{3.6}$$

In the case of the wind boundary profiles for turbulent kinetic energy, FLACS uses the equations proposed by Han et al. (2000) to calculate k and ε.

The heated air close to the ground surface causes unstable boundary layers, because the air density close to the ground is lower than the air above, generating unstableness.

For unstable boundary layers (A, B, and C), the inlet profiles are:

$$\kappa(z) = \begin{cases} 0.36w^{*2} + 0.85u^{*2}\left(1 - 3\frac{z}{L}\right)^{\frac{2}{3}} & \text{for } z \leq 0.1h \\ \left(0.36 + 0.9\left(\frac{z}{h_{abl}}\right)^{\frac{2}{3}}\left(1 - 0.8\frac{z}{h_{abl}}\right)^{2}\right)w^{*2} & \text{for } z > 0.1h \end{cases} \tag{3.7}$$

and

$$\varepsilon(z) = \begin{cases} \frac{u^{*3}}{\kappa z}\left(1 + 0.5\left|\frac{z}{L}\right|^{\frac{2}{3}}\right)^{1.5} & \text{for } z \leq 0.1h \\ \frac{w^{*3}}{h}\left(0.8 - 0.3\frac{z}{h}\right) & \text{for } z > 0.1h \end{cases} \tag{3.8}$$

The heat velocity w* is given by the next expression:

$$w^* = \left(\frac{g\dot{q}_g h_{abl}}{T_0 \rho_\infty c_p}\right)^{\frac{1}{3}} \tag{3.9}$$

For neutral and stable boundary layers; relations between friction velocity and Monin-Obukhov length are given:

$$\kappa(z) = \begin{cases} 6u^{*2} & \text{for } z \leq 0.1h \\ 6u^{*2}\left(1 - \frac{z}{h}\right)^{1.75} & \text{for } z > 0.1h \end{cases} \tag{3.10}$$

and

$$\varepsilon(z) = \begin{cases} \frac{u^{*3}}{\kappa z}\left(1.24 + 4.3\frac{z}{L}\right) & \text{for } z \leq 0.1h \\ \frac{u^{*3}}{\kappa z}\left(1.24 + 4.3\frac{z}{L}\right)(1 - 0.85z/h)^{1.5} & \text{for } z > 0.1h \end{cases} \tag{3.11}$$

3.2.2 LNG pool model

The governing equations for a spreading pool in FLACS takes into account the friction, heat and mass transfer. This model has been validated for a spreading pool with and without obstacles under different conditions: adiabatic, on water, and on soil.

For cryogenic liquids such as LNG, the heat transfer is dominated by the heat from the substrate where the pool is formed. The equation 3.12 gives the heat transfer from all types of ground at non-boiling conditions:

$$q_{g,cond} = \begin{cases} \frac{\lambda_g(T_g^{\infty} - T_p)(1.5 - 0.25(t - t_{gw}))}{\sqrt{\pi \alpha g}} & \text{if } t < 4s \\ \frac{\lambda_g(T_g^{\infty} - T_p)}{\sqrt{\pi \alpha g (t - t_{gw})}} & \text{if } t \geq 4s \end{cases} \quad (3.12)$$

Equation 3.12 is only valid for conductive heat transfer; some parameters are: α_g which is the thermal diffusivity, λ_g is the thermal conductivity, t_{gw} is the time when the pool starts, and T_g^{∞} is the ground temperature before the ground is wetted.

Besides the conductive heat transfer, there is a convective contribution between the spreading pool and the ground, which is showed in equation 3.13.

$$q_{g,conv} = 0.0133 Re_h^{0.69} Pr_l^{0.4} \frac{\lambda_l}{h} (T_g^s - T_p) \quad (3.13)$$

where:

$\lambda_{l:}$ Conductivity

$P_{rl:}$ Prandtl number of the pool liquid

T_g^s: Ground temperature at the surface.

Therefore, the total heat transfer for pools at non-boiling conditions, and on all types of ground can be calculated by using the cubic blending function:

$$q_g = (q_{g,cond}^3 + q_{g,conv}^3)^{1/3} \quad (3.14)$$

The term T_g^s given in equation 3.13 indicates the ground temperature at the surface, which can be calculated by the next equation:

$$T_g^s = T_g^\infty + 2\frac{\overline{q_s}}{\lambda_g}\sqrt{\frac{\propto_g \cdot (t - t_{gw})}{\pi}} \quad (3.15)$$

When the pool develops on smooth surfaces such as water; instead using the equations explained above, the boiling heat transfer equations are used. When the surface temperature where the pool is formed is at least 4 K higher than the boiling point temperature of the pool liquid, a phenomenon called slight superheat occurs. Nucleate boiling of a pool is assumed for slight superheats; and Cooper's correlation is used to calculate the heat transfer generated:

$$\dot{q_{s,nb}} = (55 p_r^{0.12}(-log p_r)^{-0.55} M^{-0.5}(T_g^s - T_p))^3 \quad (3.16)$$

and

$$p_r = p_{sat}/p_c \quad (3.17)$$

where:

p_{sat}: Saturation pressure

p_c: Critical pressure

Then, the nucleate boiling heat transfer is used instead of the conductive heat transfer in the cubic blending function to calculate the total heat transfer.

During the film-boiling regime, expressions for transition boiling and film boiling heat transfer are used according to (Conrado & Vesovic, 2000):

$$\dot{q_s} = \begin{cases} \dot{q_{s,film}} & \text{if } Re_h < 15 \\ \frac{1}{2}q_{s,film} + \frac{1}{2}\left(q_{s,film}\left(\frac{1500-Re_h}{1485}\right) + q_{g,conv}\left(\frac{Re_h-15}{1485}\right)\right) & \text{if } 15 \geq Re_h < 1500 \\ \frac{1}{2}\dot{q_{s,film}} + \frac{1}{2}q_{g,conv} & \text{if } Re_h \geq 1500 \end{cases} \quad (3.18)$$

where the term $\dot{q}_{g,film}$ is the film boiling heat transfer for a fluid in rest.

The convective heat transfer, based on boundary layer theory, is given by the next expression:

$$\dot{q_c} = \frac{\rho_g C_\mu^{\frac{1}{4}} k^{\frac{1}{2}} c_{p,g}(T_g - T_p)}{T^+} \quad (3.19)$$

Term T^+ is given by a two-layer model:

$$T^+ = \begin{cases} Pry^+ & \text{if } y^+ < E^+ \\ E^+ Pr + \frac{P_{rT}}{k} \ln\left(\frac{y^+}{E^+}\right) & \text{if } y^+ \geq E^+ \end{cases} \quad (3.20)$$

The convective mass transfer is given by the next expression:

$$\dot{m}_c = \frac{\rho_g C_\mu^{\frac{1}{4}} k^{\frac{1}{2}} \frac{p_0}{RT_p}(x - x_{sat})}{x^+} \quad (3.21)$$

where $x = P_g/P_0$

and x^+ is calculated by:

$$x^+ = \begin{cases} Scy^+ & \text{if } y^+ < E^+ \\ E^+ Sc + \frac{S_{cT}}{k} \ln\left(\frac{y^+}{E^+}\right) & \text{if } y^+ \geq E^+ \end{cases} \quad (3.22)$$

The radiative heat transfer caused by the contribution of the sun and surroundings can be calculated by:

$$\dot{q_{rad}} = (1 - \omega) q_{sun} + \varepsilon_g \sigma T_p^4 - \varepsilon_p \sigma T_p^4 \quad (3.23)$$

where:

w: Albedo

ε_g : Emission coefficient of the surrounding gas

ε_p: Emission coefficient of the pool liquid

Σ: Stefan-Boltzmann constant.

The total evaporation rate is given by the sum of the convective mass transfer and boiling:

$$\dot{m_V} = \dot{m_c} + \dot{m_{boil}} \tag{3.24}$$

where:

$$\dot{m_{boil}} = max\left\{\frac{q_g+q_c+q_{rad}}{\Delta h_{fg}} - m_c,\ 0\right. \tag{3.25}$$

The next equation shows the heat transfer due to evaporation:

$$q_{evap} = -(m_c + m_{boil})\Delta h_{fg} \tag{3.26}$$

3.3 VALIDATION OF FLACS AGAINST FALCON 1 TEST

Previous validation studies of Falcon tests were performed using CFD tools; for instance, FLUENT code was used to simulate the Falcon 1 test, providing some of the necessary parameters to accurately predict this test. Also, a comparison between experimental and simulation results was provided (Gavelli et al., 2008).

On the other hand, FLACS code was validated against Falcon tests using the model evaluation database for LNG vapor dispersion, showing reliable results in its prediction (Hansen et al., 2010).

For the purpose of this research, it is important to demonstrate that the results obtained by different authors with regard to the Falcon 1 test, can be replicated using FLACS. By doing this, it can be inferred that the model is reliable and can be applied to other scenarios involving LNG releases.

This section is going to develop the validation for the Falcon 1 test using FLACS, and the results obtained are going to be compared with previously reported results in FLUENT (Gavelli et al., 2008).

3.3.1 Computational geometry and meshing

The Falcon 1 test considered an LNG release inside a water pond surrounded by vapor fences and a billboard structure located upwind. The details of this experiment were explained in detail in Chapter I.

The simulation domain considered the x axis as horizontal and parallel to the wind direction, y axis as horizontal in the crosswind direction, and the z axis as vertical. The origin point was located in the center of the downwind fence, at ground level.

The computational domain considered ranges from -200 m to 300 m in the x-direction, from -250 m to 250 m in the y-direction, and from 0 m to 50 m in the z-direction.

Water pond, vapor fences, and the billboard were included in the model to take into account their effects in vapor dispersion. Figure 3.1 shows the computational geometry generated in FLACS for the Falcon 1 test.

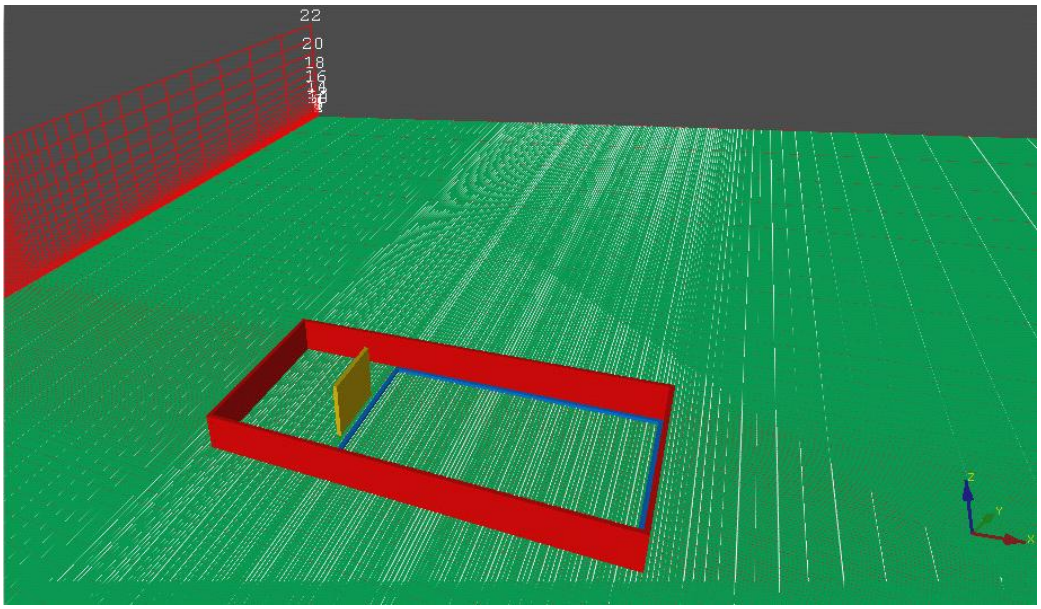

Fig. 3.1. Computational geometry generated in FLACS for Falcon 1 test

Meshing process was performed on the domain, with a grid refinement close to the pool leak and the obstacles considered in the set up.

The total control volumes were 382,000; with Cartesian grid cells about 0.8 x 0.8 x 0.5 m in the refinement zone. Figure 3.2 shows the details of the meshing and refinement on the simulation domain.

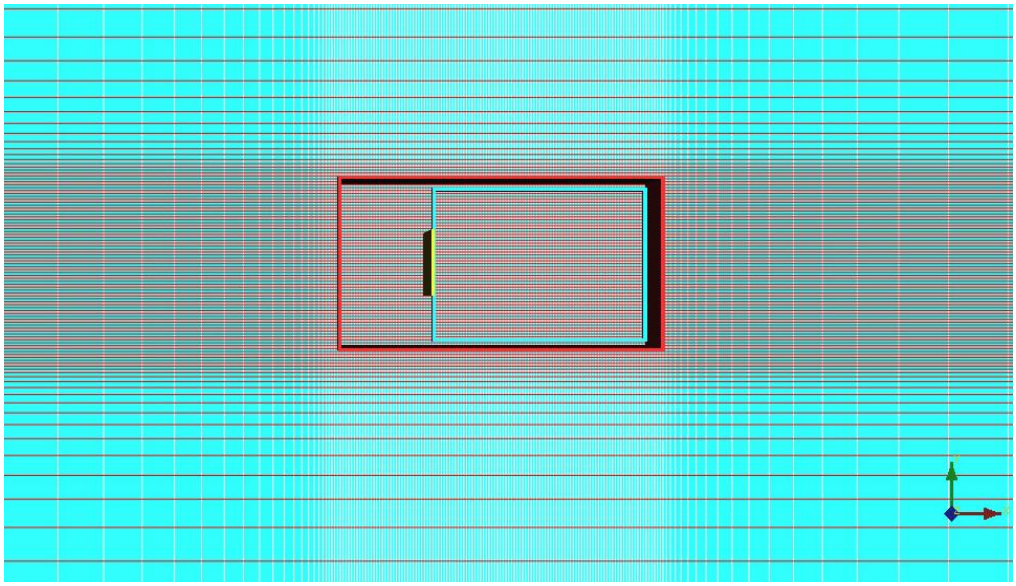

Fig. 3.2. Detail of meshing and refinement on the simulation domain

3.3.2 Simulation set up

Monitor points for measuring vapor concentration were located downwind the vapor fence, using the same location as in the Falcon 1 experiment. Boundary conditions, which are a set of differential equations at the boundary of a given domain,

were considered for the outlet simulation domain. Wind inflow boundary was assumed in the x direction (upwind from the vapor fence) and along the y direction. Nozzle condition was considered for the outflow boundary in the x direction (downwind from the vapor fence), and also on the top of z direction.

As initial conditions, wind velocity of 1.7 m/s measured at 2 m height. Pasquill stability class "D" and an ambient temperature of 32.8 ºC were selected. The aerodynamic roughness length (z_0) was 0.03, similar to typical values for flat terrain.

FLACS pool model was used to calculate the pool formed during the LNG spill and the vaporization rate generated from it. LNG with a composition of 95% methane, 4% ethane and 1% propane was released inside the water pond with a spill rate of 202 kg/s, during a total time of 131 s. The model takes turbulence caused by the LNG discharge into consideration by a relative turbulence intensity of 0.05, similar to medium turbulence intensity.

3.3.3 Simulation results

Comparison between the experimental data in Falcon test 1 and the results obtained with FLUENT (Gavelli et al., 2008) and FLACS (this work) are shown in Figure 3.3.

The continuous blue line represents the experimental data, while the FLUENT simulation result is shown by the profile green line. The FLACS simulation result obtained in this research is shown by the continuous black line.

The results obtained with FLACS indicated that the cloud pass over the fence at approximately a time of 70 s, when it reaches the analyzed concentration measurement point. Afterwards, the concentration will build up until it reaches 7.5% v/v at a time of 260 s, and then it finally decreases.

Both models (FLACS and FLUENT) showed the same pattern and they are reasonable accurate despite the under-prediction in the simulation results. The reason for this under-prediction was the peculiar release conditions during the Falcon 1 experiments, where a high pressure jet was observed, with associated flashing and aerosol formation. Therefore, it is concluded that the difference between experimental and simulation results are given because the definition of the source term, rather than a deficiency with the model.

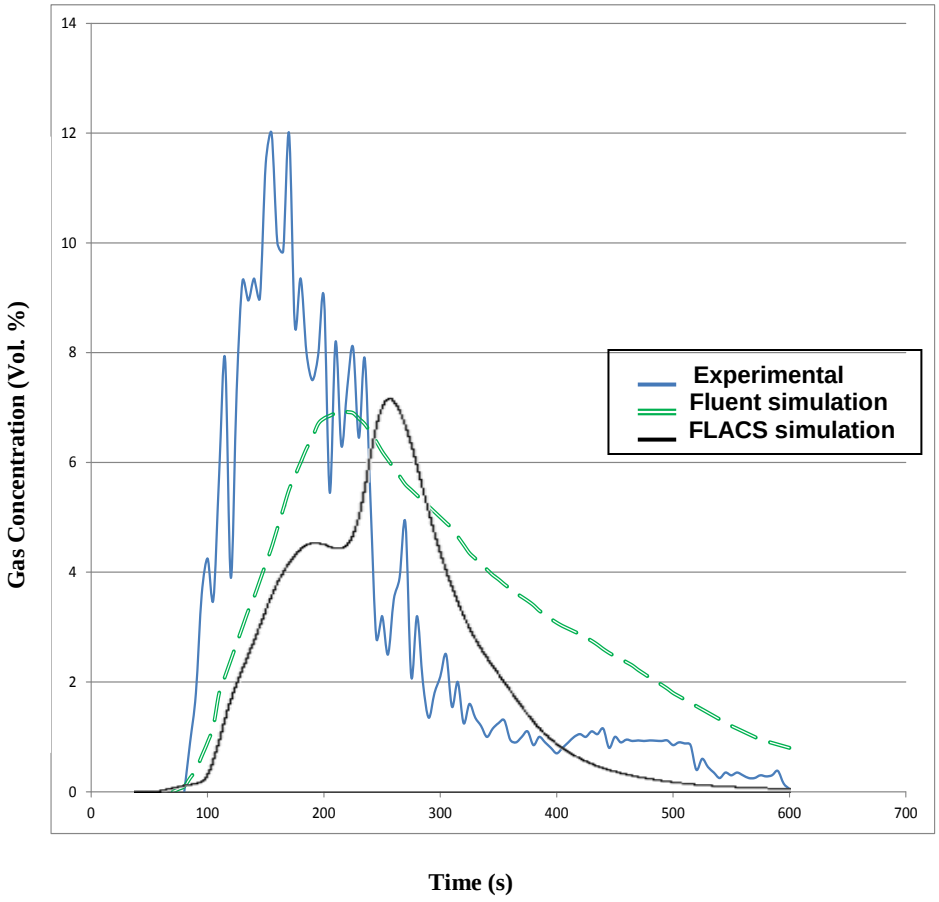

Fig. 3.3. FLACS validation against experimental data and FLUENT simulation

CHAPTER IV

PARAMETRIC ANALYSIS AND SIMULATION

The first chapter explained that vapor dispersion modeling includes two main phenomena: the source term and vapor dispersion. This research is focused on the vapor dispersion and the effects of the key parameters in reducing the concentration values by enhancing mixing of LNG vapor with air. Five key parameters were selected and studied: height, width, and shape of the obstacles as well as ground roughness and wind velocity (Cormier, 2008).

This chapter is divided in two main sections: vapor cloud behavior under different parameters, and parametric analysis. The first section explains the different behavior that a vapor cloud when a variation in the parameters mentioned above is performed. The second section discusses the parametric analysis performed on the analyzed parameters and finds the parameters contribution in the concentration reduction.

4.1 SIMULATION SETUP

Previous wind tunnel experiments studied the behavior and dispersion of heavier-than-air gases passing through two main obstacles: cube and vertical cylinder (Mavroidis et al., 2003). Although LNG was not used for these experiments, its properties are comparable to a heavier-than-air gas; therefore, a similar behavior can be expected.

Inside an LNG facility, for instance an LNG terminal, the main obstacles that can be found are buildings and tanks, which for simulation purposes can be generalized as cubes and cylinders, respectively. The effects that these obstacles may have over an LNG vapor dispersion scenario are going to be analyzed by using FLACS code. The setup for the simulation analysis is similar to the wind tunnel experiments developed by Mavroidis in 2003, and explained in Chapter I.

The release source was located upwind from the analyzed obstacles, at a distance 2 times larger than their width, which for these simulations was 3 meters. In the same manner, concentration measurement points were considered downwind from the rear face of the obstacle, and located at distances 2 times their width, as observed in Figure 4.1.

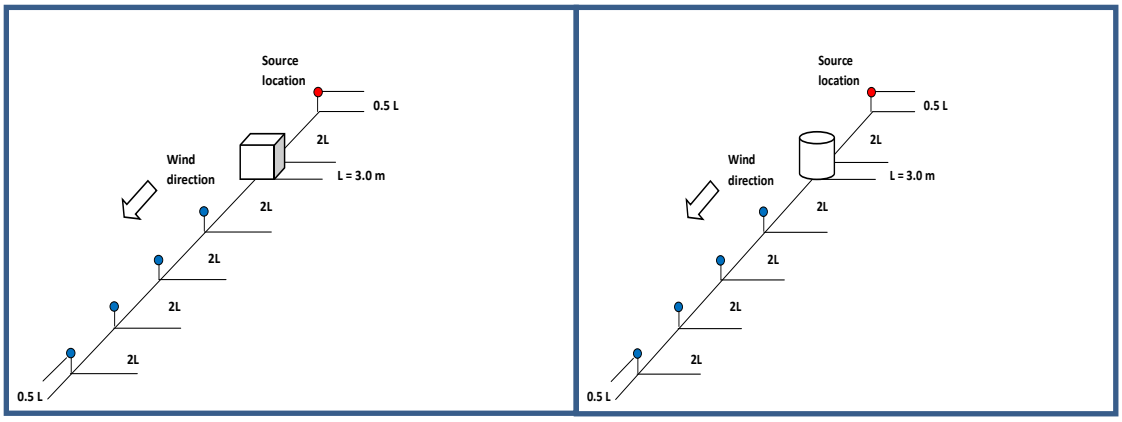

(a) **(b)**

Fig. 4.1. Location of the source and measurement points for gas concentration in the cases of: cube (a) and cylinder (b).

4.2 VAPOR CLOUD BEHAVIOR ON DIFFERENT PARAMETERS

For this analysis a base case scenario was considered, with continuous gas release rate of 4.5 kg/s initiated at the source point, as indicated in Figure 4.1. FLACS diffuse model was used for the simulations, because it allows a release with low momentum and velocity, similar to the gas release characteristics in wind tunnels. Neutral stability conditions were considered with a low wind velocity of 1.5 m/s, and ground roughness value of 0.03.

4.2.1 Shape effect

The effect that shape of the obstacles plays on the vapor dispersion was evaluated by analyzing two different obstacles: cylinder and cube. The simulation results for these obstacles are shown in Figure 4.2. This figure shows the contours of the flammable region with a gas concentration from the ½ Lower Flammability Limit (LFL) to the Upper Flammability Limit (UFL). For LNG vapor the LFL and UFL values are 5 and 15% by volume, respectively. At time t= 180 seconds, it can be seen that the concentration values downwind from both the cube and cylinder along the centerline are lower than the ½ LFL value, falling out the flammability region. This region is plotted with no color, and it is more pronounced for the case of the cube compared with the cylinder. The reason for this behavior is because cylinders and cubes produce different flow patterns, causing a faster reattachment of the cloud in the case of cylinder, after the gas cloud passed through it

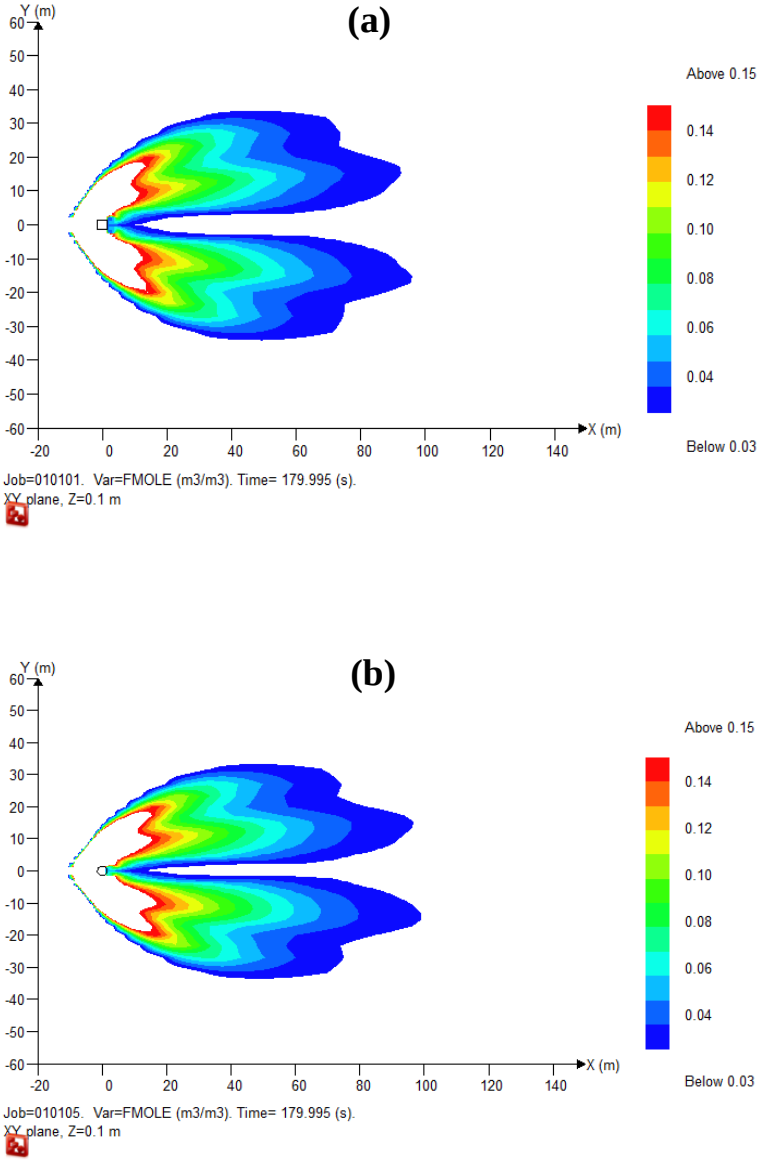

Fig. 4.2. Shape effect on vapor cloud for cube (a) and cylinder (b).

Figure 4.3 compares concentration values obtained with the cylinder and cube obstacles at different distances (in meters) downwind from the obstacles at t= 180 seconds.

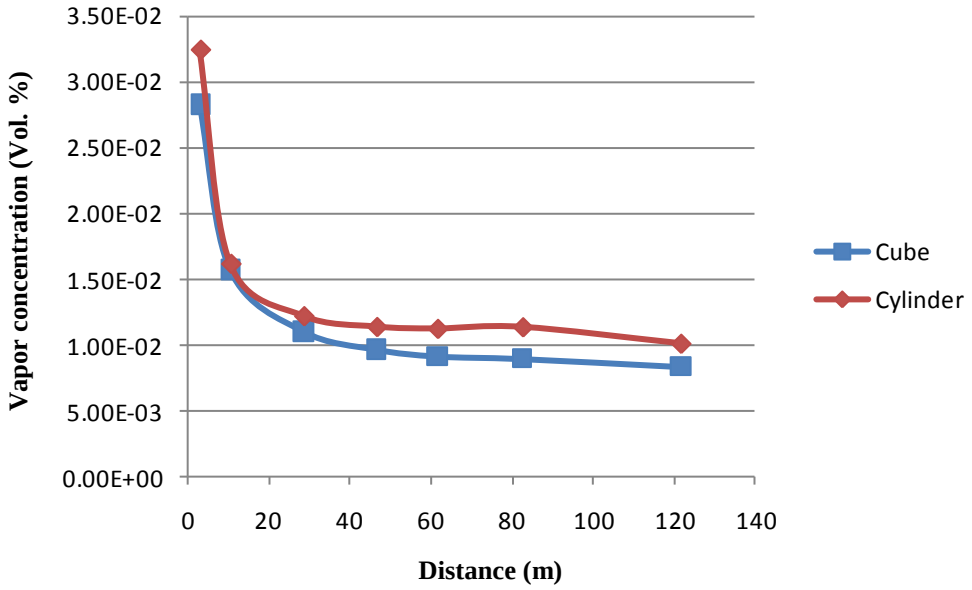

Fig. 4.3. Concentration values along the centerline for cube and cylinder.

4.2.2 Height effect

In this case, the height of the obstacles was increased from 3 meters to 6 meters; however, the width was kept constant at 3meters. Figure 4.4 shows the flammable region contours of the vapor cloud for the cube case. The wider region (with no color) downwind from the cube indicates that the concentration values along the centerline were decreased by augmenting the height of the cube.

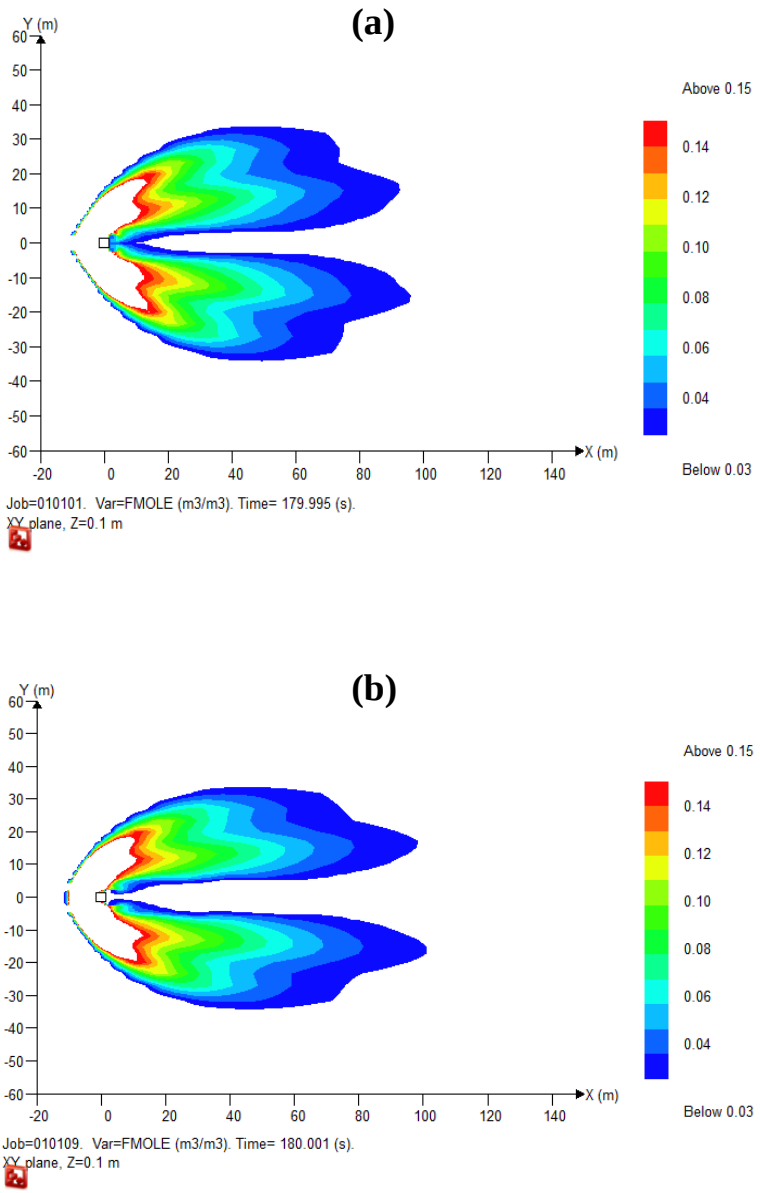

Fig. 4.4. Height effect on vapor cloud for a 3m cube (a) and increased height of cube to 6m (b).

Figure 4.5 shows the concentration values and the concentration reduction (in percentage) along the centerline, for the cube and cylinder obstacles. In this case, the concentration values were decreased by 90% for the cube, while for the cylinder this reduction was 85%.

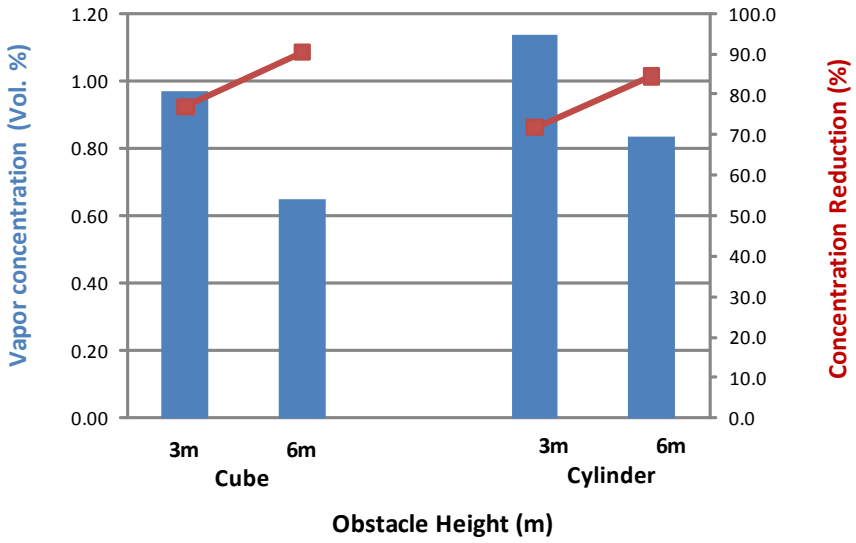

Fig. 4.5. Concentration values and reduction efficiency for cube and cylinder.

4.2.3 Width effect

Modification in the obstacles was done by doubling their width from 3m to 6m, but keeping the height at 3m. A similar behavior as the previous case was obtained. Figure 4.6 shows the comparison between the flammable regions of the vapor clouds, for the cube case. It is concluded that an increment in the width of the obstacle results in a

decrement in the concentration values along the centerline, as indicated by the region with no color downwind from the cube.

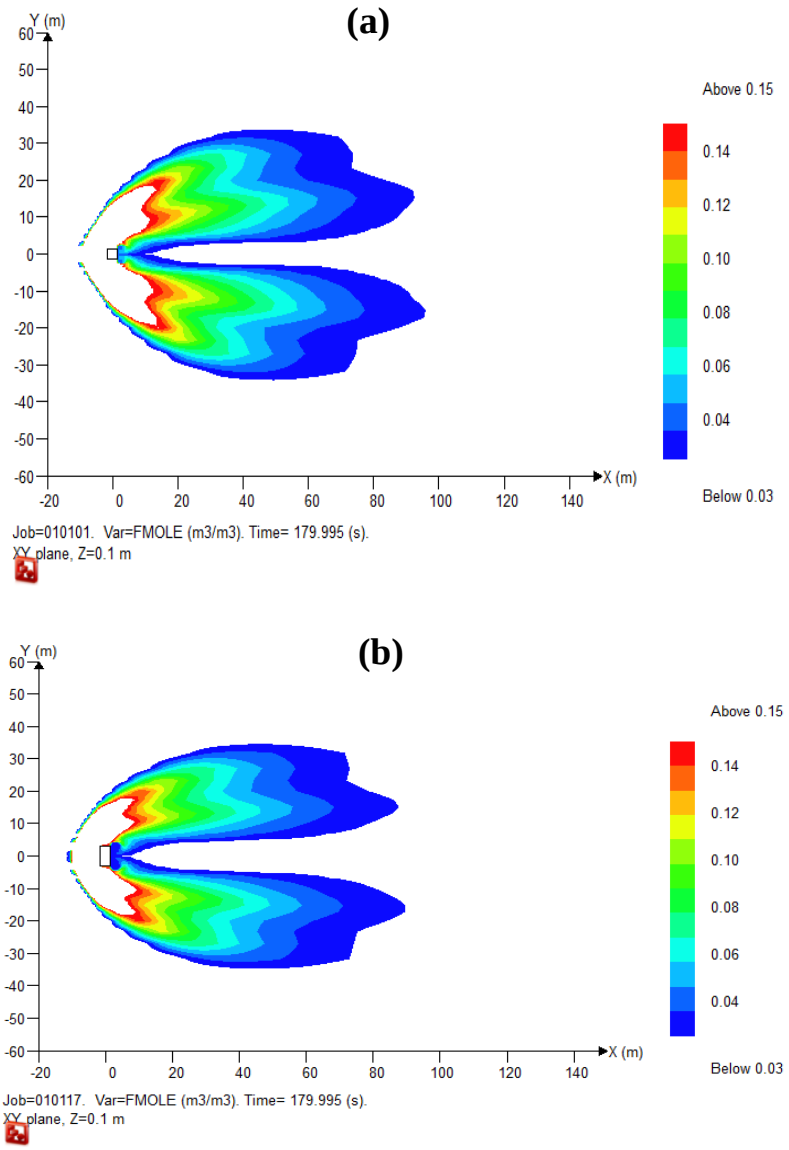

Fig. 4.6. Width effect on vapor cloud for a 3m cube (a) and increased width of cube to 6m (b).

Figure 4.7 shows the concentration values and concentration reduction (in percentage) along the centerline for the cube and cylinder cases. The concentration reduction was 84.5 % for the cylinder and 82.6 % for the cube.

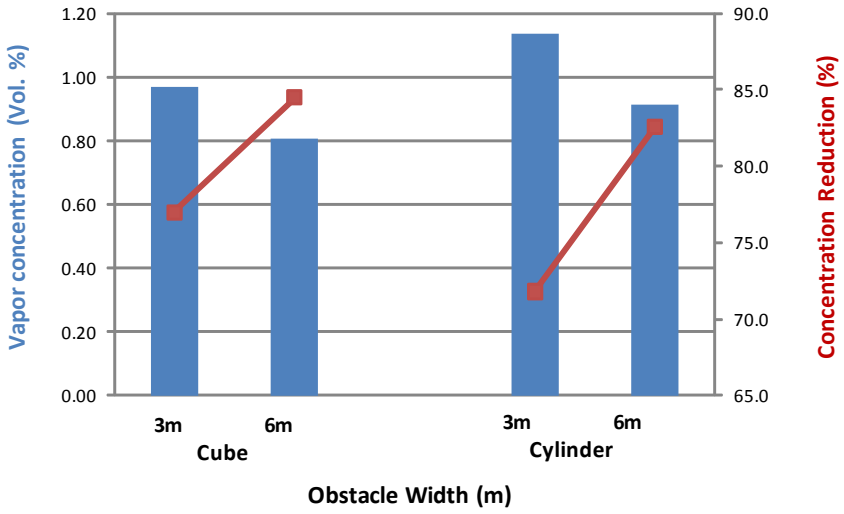

Fig. 4.7. Concentration values and concentration reduction for cube and cylinder with increased width.

4.2.4 Roughness effect

Roughness is an important parameter in vapor dispersion, because a large homogeneous roughness can considerably reduce the concentration values downwind (Petersen, 1990). In this case, Figure 4.8 (a) shows the flammable contours for the vapor cloud with a roughness value of 0.0002 and (b) with a roughness value of 0.03. The

concentration reduction values are noticeably decreased not only along the centerline, but also in the dimensions of the cloud. For this case the safety distance (½ LFL) was reduced from 90 meters to 50 meters approximately.

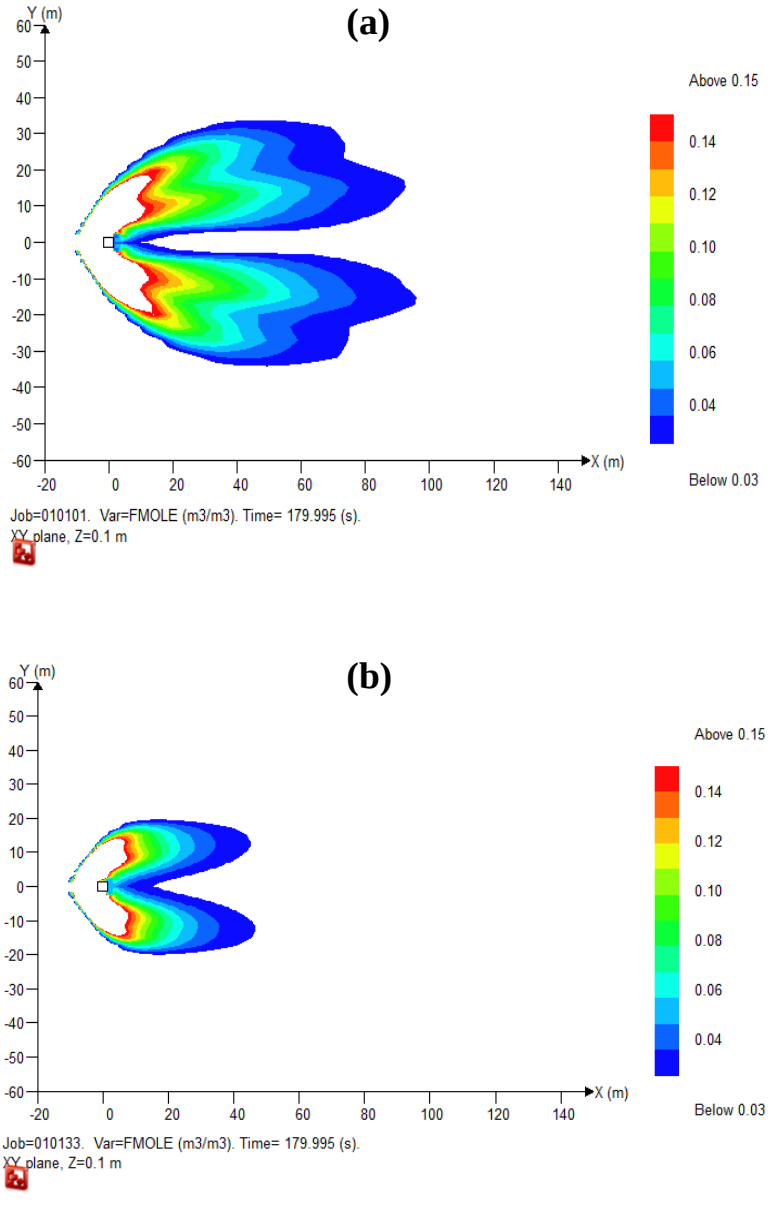

Fig. 4.8. Cloud shape for cube with roughness 0.0002 (a) and roughness 0.03 (b).

Figure 4.9 shows the concentration values and the reduction efficiency along the centerline for the cube and cylinder cases. For the cube, a concentration reduction of 85 % was obtained and for the cylinder this reduction was 80 % when surface roughness was increased from 0.0002 to 0.03.

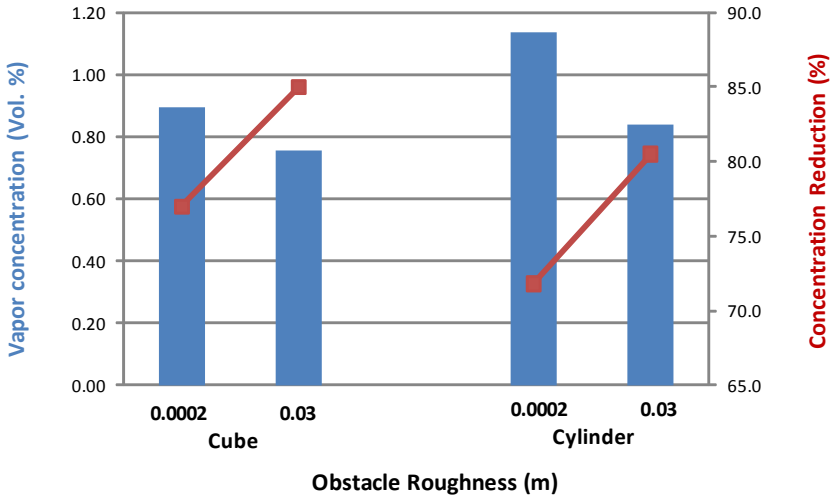

Fig. 4.9. Concentration values and concentration reduction for cube and cylinder with different roughness values.

4.2.5 Wind velocity effect

Also it is important to analyze other parameters unrelated to the geometry of the obstacles such as the wind velocity. Figure 4.10 shows the effect of wind velocity over the vapor dispersion for the cube case. A noticeable reduction in the width of the flammable region is found, and also along the centerline downwind from the cube when

the wind velocity was 6 m/s. However, there also are some traces of flammable mixture on the sides, caused by the separation of the cloud after it passed through the cube.

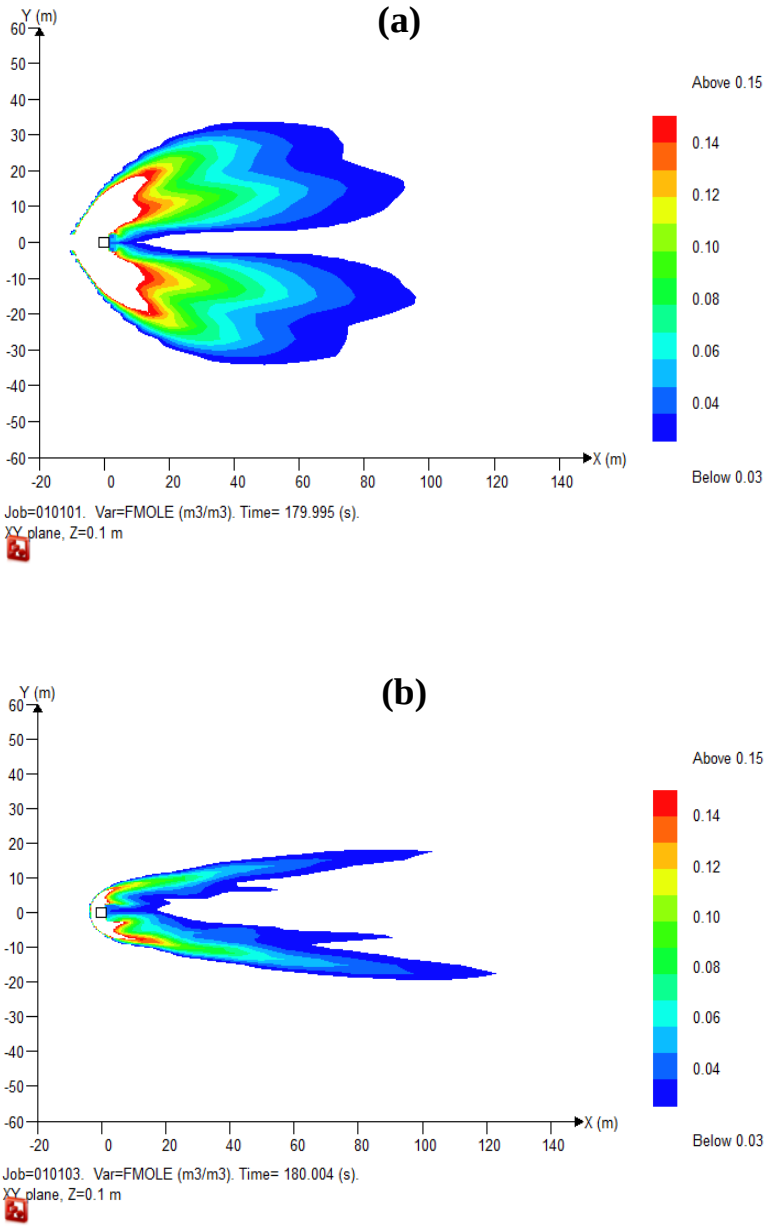

Fig. 4.10. Wind velocity effect for a velocity of 1.5 m/s (a) and 6 m/s (b).

4.3 PARAMETRIC ANALYSIS

The previous analysis allowed us to understand the effect of a single parameter on LNG vapor behavior; however, not a combined effect of all of them. Parametric analysis allows combining all the levels involved in the vapor dispersion through obstacles, investigating the effects of each simple factor (parameter) and also the interaction of them; therefore, it is possible to find the joint effect of the factors on a given response (Montgomery & Runger, 2006). Different factors that will be investigated in this section are the same as discussed earlier: height, width, geometry shape, surface roughness and wind speed.

A special case of 2k factorial design is used in this research. In this design, k represents the five factors discussed earlier, and they are analyzed at two levels. The 2k factorial design is applied to two accidental scenarios. In first of these, LNG spilled onto the ground and pool formation was assumed. In the second scenario an LNG jet was released. The resulting amounts of simulations were 32 for each case, and they were compared with a case of dispersion without obstacles, in order to know the difference in concentration reduction.

Tables 4.1 and 4.2 list all the 32 runs for the pool and jet release cases, respectively. The symbols – 1 and + 1 represent the low and high levels of the factors; the table also shows the concentration values without obstacles and with obstacles at 3 m and 82.5 m downwind the obstacles. Efficiency in concentration reduction also is showed for these points.

Table 4.1 Simulation details for parametric analysis in pool release case

Run	Wind	Shape	Height	Width	Roughness	Concentration with no obstacle		Concentration with obstacle		Reduction Efficiency (%)	
						x = 3m	x = 82.5m	x = 3m	x = 82.5 m	Effic. (x=3m)	Effic. (x=82.5m)
1	-1	-1	-1	-1	-1	0.1786	0.0519	0.0410	0.0107	77.0	79.5
2	1	-1	-1	-1	-1	0.5648	0.0268	0.0405	0.0119	92.8	55.6
3	-1	1	-1	-1	-1	0.1786	0.0519	0.0503	0.0154	71.8	70.3
4	1	1	-1	-1	-1	0.5648	0.0268	0.1298	0.0119	77.0	55.6
5	-1	-1	1	-1	-1	0.1786	0.0519	0.0172	0.0061	90.4	88.2
6	1	-1	1	-1	-1	0.5648	0.0268	0.0325	0.0078	94.2	70.8
7	-1	1	1	-1	-1	0.1786	0.0519	0.0279	0.0081	84.4	84.3
8	1	1	1	-1	-1	0.5648	0.0268	0.0292	0.0082	94.8	69.4
9	-1	-1	-1	1	-1	0.1786	0.0519	0.0277	0.0078	84.5	85.0
10	1	-1	-1	1	-1	0.5648	0.0268	0.0410	0.0204	92.7	23.8
11	-1	1	-1	1	-1	0.1786	0.0519	0.0311	0.0118	82.6	77.2
12	1	1	-1	1	-1	0.5648	0.0268	0.0463	0.0095	91.8	64.7
13	-1	-1	1	1	-1	0.1786	0.0519	0.0073	0.0036	95.9	93.1
14	1	-1	1	1	-1	0.5648	0.0268	0.0064	0.0032	98.9	87.9
15	-1	1	1	1	-1	0.1786	0.0519	0.0103	0.0046	94.2	91.2
16	1	1	1	1	-1	0.5648	0.0268	0.0079	0.0032	98.6	88.0
17	-1	-1	-1	-1	1	0.1912	0.0134	0.0498	0.0086	85.0	95.3
18	1	-1	-1	-1	1	0.4784	0.0385	0.0448	0.0113	90.6	70.5
19	-1	1	-1	-1	1	0.1912	0.0134	0.0579	0.0098	80.5	93.0
20	1	1	-1	-1	1	0.4784	0.0385	0.1134	0.0146	76.3	62.1
21	-1	-1	1	-1	1	0.1912	0.0134	0.0263	0.0073	86.3	45.1
22	1	-1	1	-1	1	0.4784	0.0385	0.0192	0.0021	96.0	94.6
23	-1	1	1	-1	1	0.1912	0.0134	0.0326	0.0089	82.9	33.6
24	1	1	1	-1	1	0.4784	0.0385	0.0398	0.0042	91.7	89.2
25	-1	-1	-1	1	1	0.1912	0.0134	0.0261	0.0068	86.3	49.0
26	1	-1	-1	1	1	0.4784	0.0385	0.0144	0.0043	97.0	88.8
27	-1	1	-1	1	1	0.1912	0.0134	0.0329	0.0078	82.8	41.6
28	1	1	-1	1	1	0.4784	0.0385	0.0375	0.0054	92.2	86.0
29	-1	-1	1	1	1	0.1912	0.0134	0.0095	0.0047	95.0	65.1
30	1	-1	1	1	1	0.4784	0.0385	0.0006	0.0003	99.9	99.2
31	-1	1	1	1	1	0.1912	0.0134	0.0095	0.0052	95.0	60.7
32	1	1	1	1	1	0.4784	0.0385	0.0022	0.0010	99.5	97.4

Table 4.2 Simulation details for parametric analysis in jet release case

	Wind	Shape	Height	Width	Roughness	Concentration no obstacle		Concentration with obstacle		Reduction Efficiency (%)	
						x = 3m	x = 82.5m	x = 3m	x = 82.5 m	Effic. (x=3m)	Effic. (x=82.5m)
1	-1	-1	-1	-1	-1	0.0935	0.0276	0.0199	0.0060	78.8	78.3
2	1	-1	-1	-1	-1	0.0733	0.0343	0.0321	0.0085	56.2	75.2
3	-1	1	-1	-1	-1	0.0935	0.0276	0.0863	0.0327	7.7	-18.4
4	1	1	-1	-1	-1	0.0733	0.0343	0.0625	0.0230	14.8	33.0
5	-1	-1	1	-1	-1	0.0935	0.0276	0.0323	0.0169	65.5	38.9
6	1	-1	1	-1	-1	0.0733	0.0343	0.0246	0.0051	66.4	85.2
7	-1	1	1	-1	-1	0.0935	0.0276	0.0791	0.0328	15.5	-18.9
8	1	1	1	-1	-1	0.0733	0.0343	0.0627	0.0315	14.5	8.2
9	-1	-1	-1	1	-1	0.0935	0.0276	0.0169	0.0061	81.9	77.9
10	1	-1	-1	1	-1	0.0733	0.0343	0.0265	0.0054	63.8	84.2
11	-1	1	-1	1	-1	0.0935	0.0276	0.0325	0.0134	65.2	51.5
12	1	1	-1	1	-1	0.0733	0.0343	0.0353	0.0159	51.9	53.5
13	-1	-1	1	1	-1	0.0935	0.0276	0.0126	0.0078	86.5	71.9
14	1	-1	1	1	-1	0.0733	0.0343	0.0104	0.0056	85.9	83.6
15	-1	1	1	1	-1	0.0935	0.0276	0.0353	0.0104	62.2	62.3
16	1	1	1	1	-1	0.0733	0.0343	0.0199	0.0083	72.9	75.8
17	-1	-1	-1	-1	1	0.0914	0.0282	0.0226	0.0064	75.3	77.3
18	1	-1	-1	-1	1	0.0743	0.0357	0.0309	0.0092	58.4	74.1
19	-1	1	-1	-1	1	0.0914	0.0282	0.0844	0.0339	7.6	-20.1
20	1	1	-1	-1	1	0.0743	0.0357	0.0624	0.0200	15.9	44.1
21	-1	-1	1	-1	1	0.0914	0.0282	0.0221	0.0079	75.8	72.0
22	1	-1	1	-1	1	0.0743	0.0357	0.0307	0.0036	58.7	89.9
23	-1	1	1	-1	1	0.0914	0.0282	0.0794	0.0340	13.2	-20.4
24	1	1	1	-1	1	0.0743	0.0357	0.0669	0.0219	10.0	38.7
25	-1	-1	-1	1	1	0.0914	0.0282	0.0187	0.0071	79.5	74.9
26	1	-1	-1	1	1	0.0743	0.0357	0.0228	0.0063	69.3	82.3
27	-1	1	-1	1	1	0.0914	0.0282	0.0370	0.0146	59.6	48.4
28	1	1	-1	1	1	0.0743	0.0357	0.0418	0.0132	43.7	63.2
29	-1	-1	1	1	1	0.0914	0.0282	0.0127	0.0067	86.1	76.1
30	1	-1	1	1	1	0.0743	0.0357	0.0093	0.0052	87.5	85.5
31	-1	1	1	1	1	0.0914	0.0282	0.0299	0.0126	67.3	55.4
32	1	1	1	1	1	0.0743	0.0357	0.0184	0.0081	75.2	77.3

The maximum and minimum values for each analyzed parameter are shown in Table 4.3. These values were selected according with worst case and most favorable case scenarios.

Table 4.3 Parameter values for pool and jet releases

Parameter	Min (-)	Max (+)
Wind	1.5 m/s	6 m/s
Shape	Cube	Cylinder
Height	3.0 m	6 m
Width	3.0 m	6 m
Roughness	0.0002	0.03

4.3.1 Analysis of pool release case

This research uses a statistical experimental design tool called Design Expert 8.7 for statistical analysis. Figure 4.11 shows a Pareto chart, the result of statistical analysis for LNG pool scenario. Here the objective was to determine the significant effect of each parameter and their combination in reducing downwind concentration of LNG vapor.

Pareto chart ranks the effects of the parameters by their magnitude, as a multiple of the standard deviation (t-value). This chart provides confidence about the significant effects of the parameters (non-zero); for instance, values above the t-Value limit provide a 95% confidence that certain effects are possibly significant, while values below the t-Value limit are not likely to be significant. The Bonferroni limit (red line in Pareto chart)

approaches to a 95% confidence level; therefore, the effects sufficiently large will pass this limit and they are almost certainly significant (DeLoach & Ulbrich, 2008).

Generally, it was observed that the height and width of the obstacles compared to other factors play a more significant role in reducing LNG concentration downwind and enhancing the turbulence when vapor is mixing with the air.

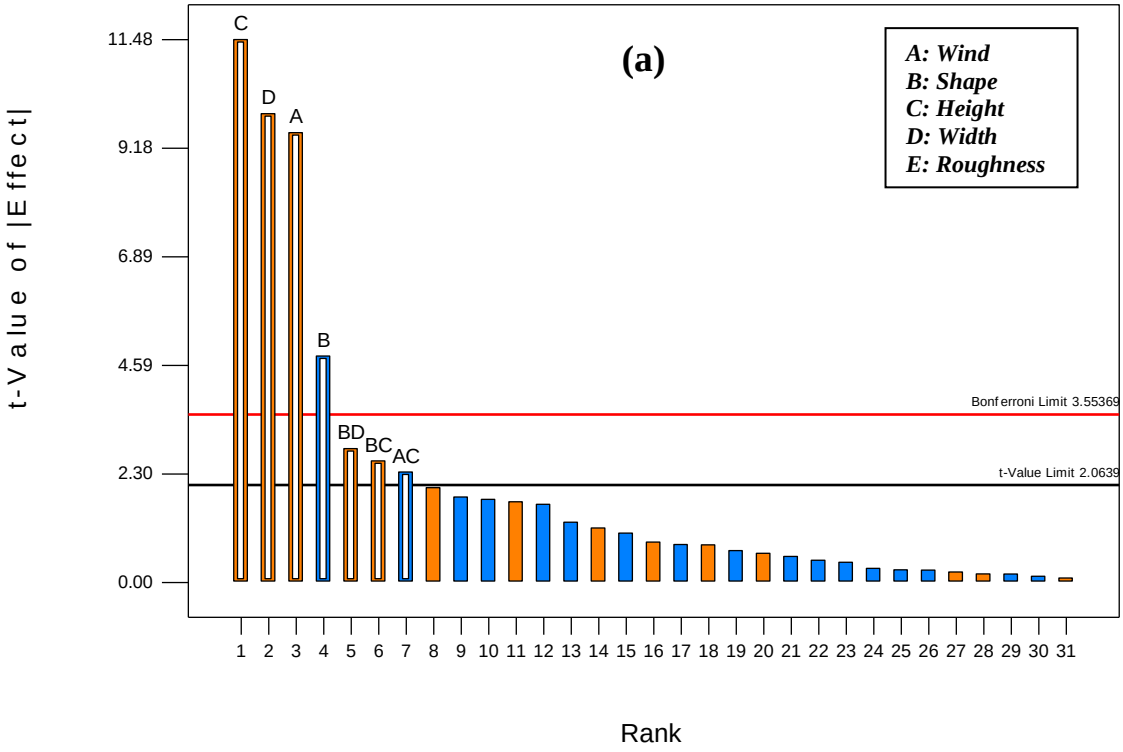

Fig. 4.11(a). Pareto chart with effects and significance of parameters at downwind distance: x = 3 m

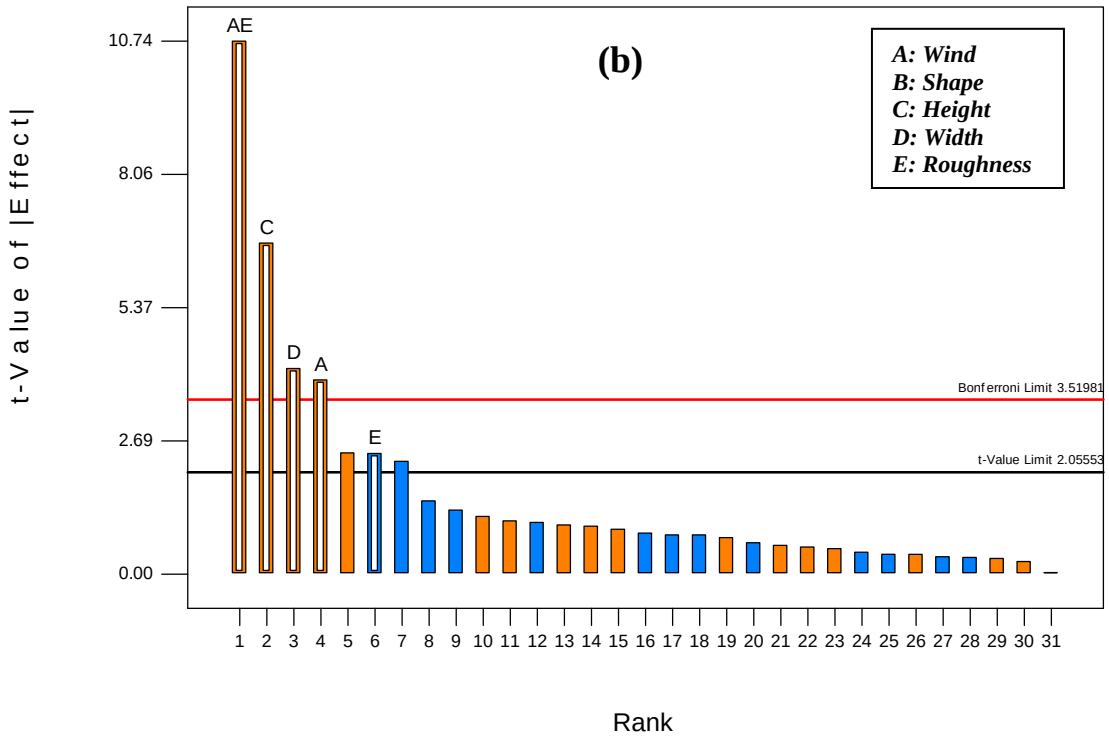

Fig. 4.11(b). Pareto chart with effects and significance of parameters at downwind distance: x = 82.5 m

From Figure 4.11(a) it is founded that the height, width, and wind velocity, play the most important role in the reduction of the vapor concentration, close to the obstacle (at 3m). When the concentration measurement is done far away point from the obstacle (at 82.5 m), a combination effect of wind velocity and ground roughness becomes more important, as can be seen in Figure 4.11 (b).

Table 4.4 shows the effect list of the parameters analyzed and their contribution in the concentration reduction at 3 m and 82.5 m downwind from the obstacle.

Table 4.4 Parameter contribution in the concentration reduction for pool release case at distances: x = 3 m and x = 82.5 m

Parameter	**Contribution in the concentration reduction (%)**	
	x= 3m	**x = 82.5m**
Height	34	19.8
Width	25.4	7.7
Wind Velocity	23.3	6.8
Shape	5.9	0.5
Roughness	0.1	2.6
Wind Velocity&Roughness	0.2	51.4
Other parameters combination	11.2	11.1

Reduction of vapor concentration values by interaction between two parameters can be better understood by using surface plots. For instance, Figure 4.12 (a) shows the efficiency in concentration reduction (in percentage) when the wind velocity or height of the obstacle were modified. By increasing, either wind velocity or height, the concentration values can be reduced by about 91%. However, if both parameters are increased at the same time, a reduction of 97% could be achieved. Figure 4.12 (b) shows the interaction between height and width of an obstacle. The values were measured at 3m from the rear face of the analyzed obstacle.

In the same manner, Figure 4.13 shows the efficiency in concentration reduction by the interaction between other main parameters: wind velocity vs. roughness (a), and width vs. height (b), at a downwind distance x =82.5 m.

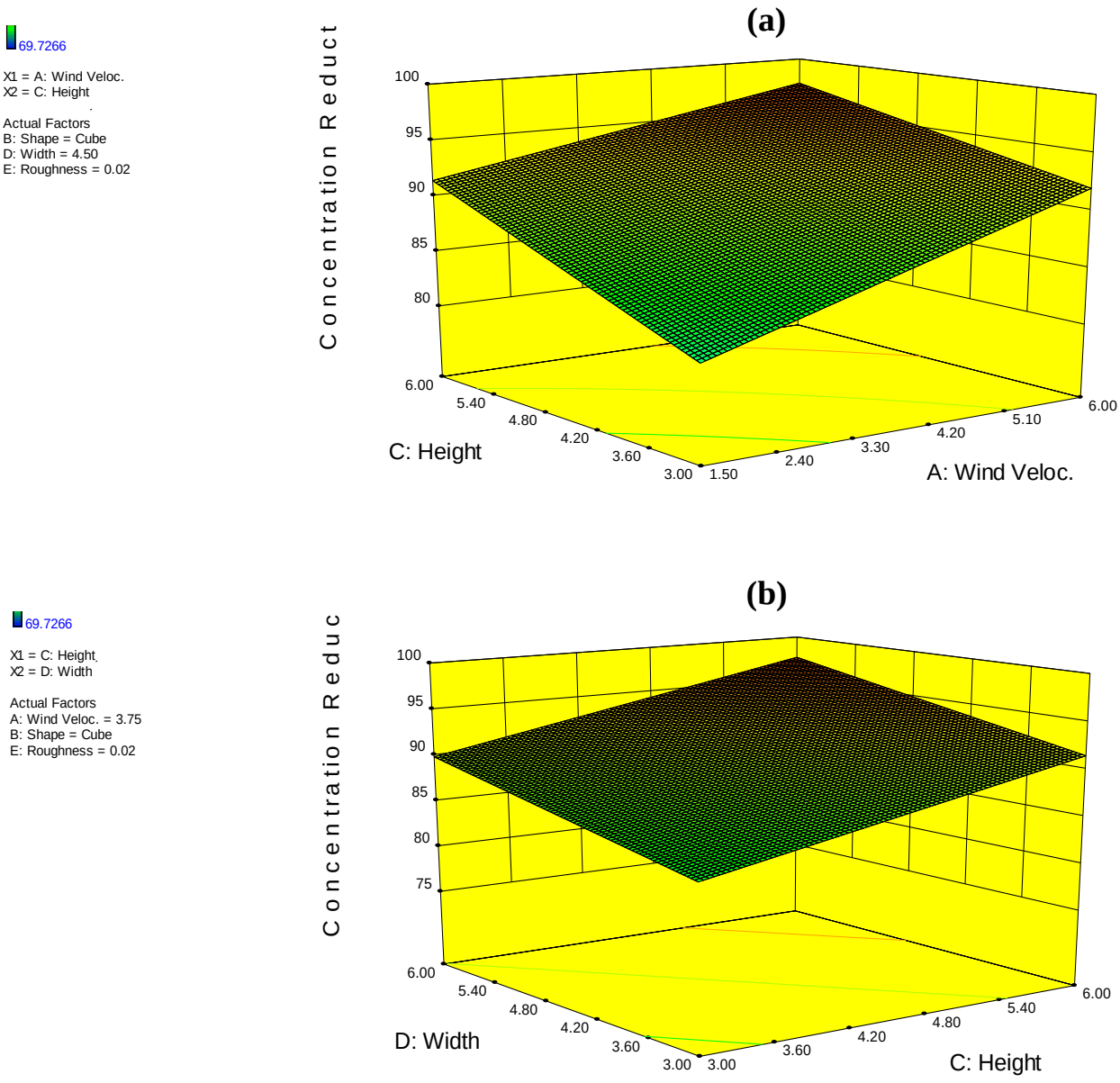

Fig. 4.12. Surface plots of parameter interaction at distance: x = 3 m

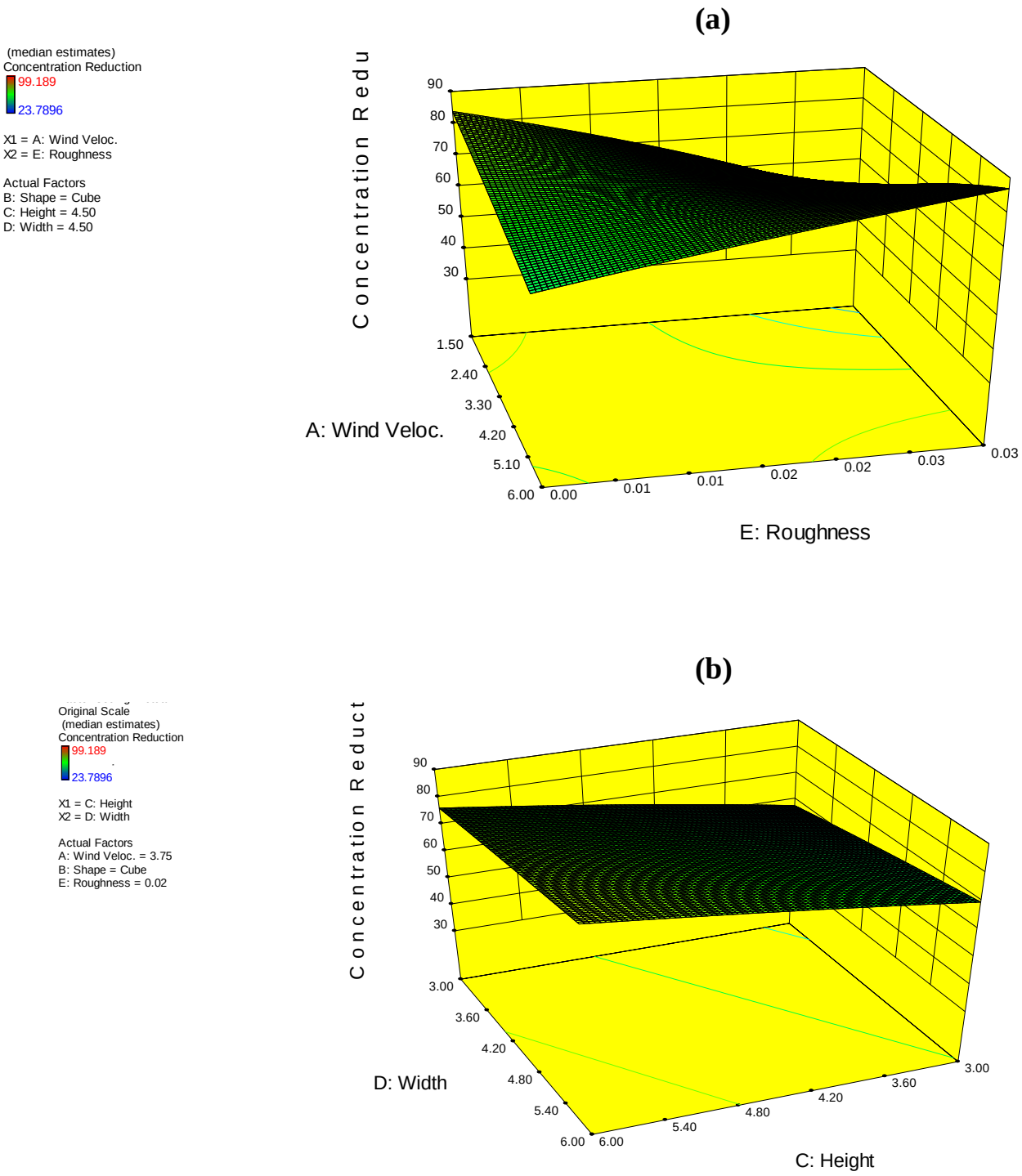

Fig. 4.13. Surface plots of parameter interaction at distance: x = 82.5 m

4.3.2 Analysis of jet release case

A similar approach as described above was used for the jet release case. The effects and significance of the parameters at a distance of 3 m and 82.5 m downwind the obstacles are shown in Figure 4.14, using Pareto charts.

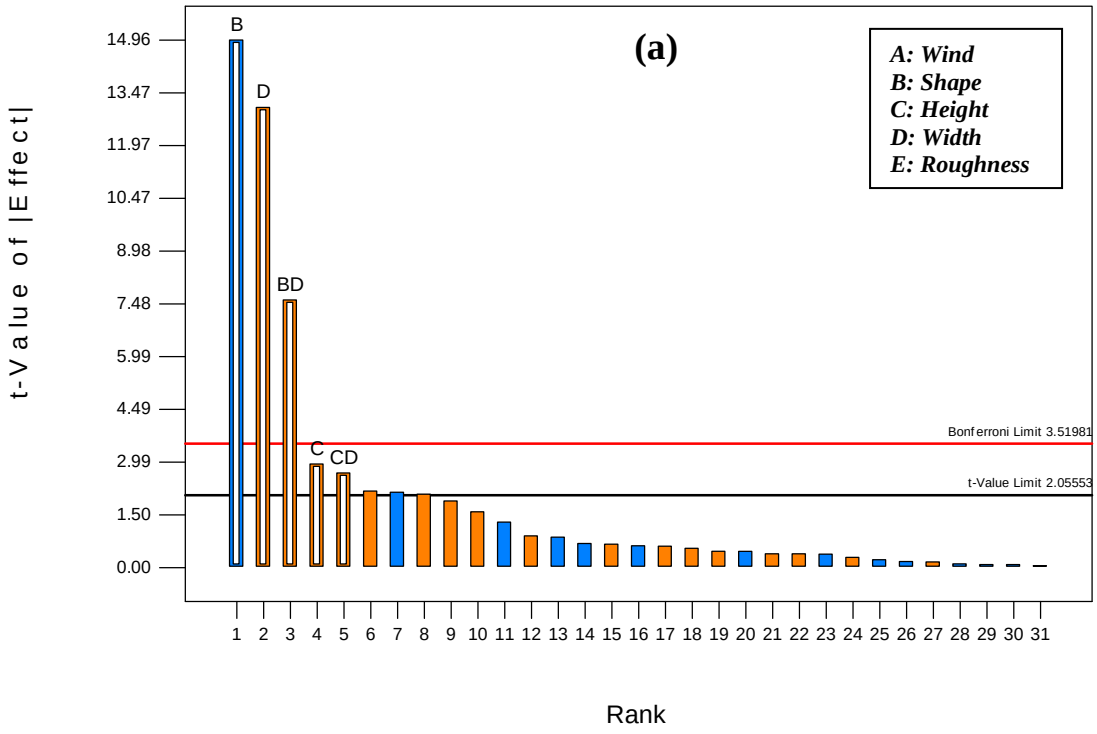

Fig. 4.14 (a). Pareto chart with effects and significance of parameters at downwind distance: x = 3 m.

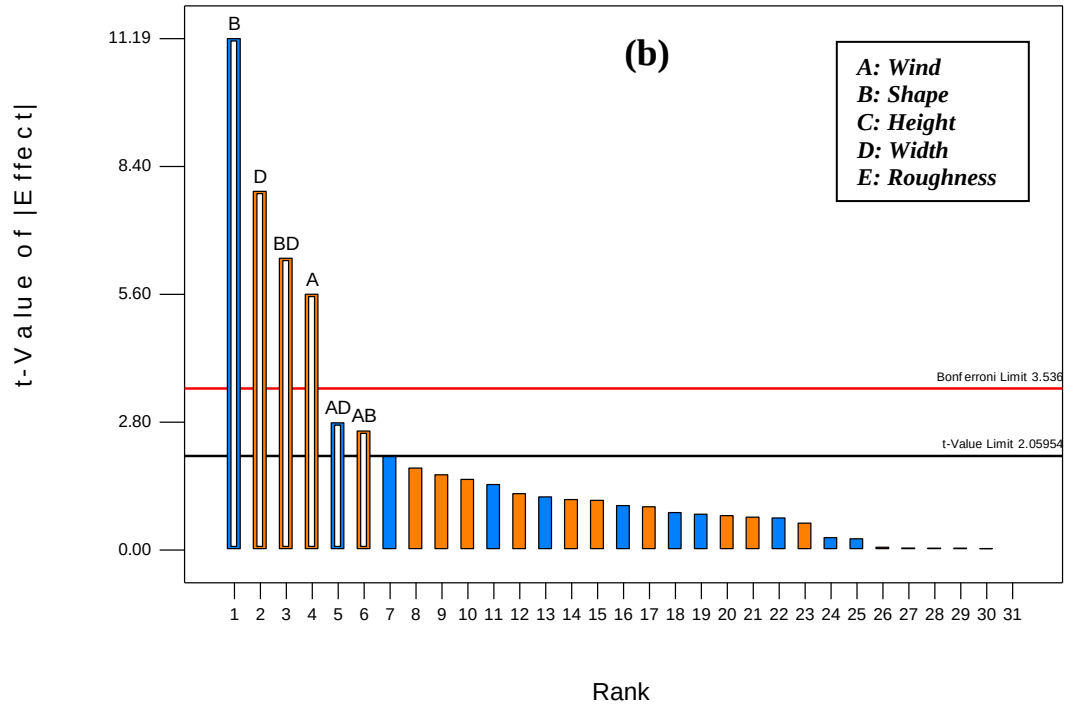

Fig. 4.14 (b). Pareto chart with effects and significance of parameters at downwind distance: x = 82.5 m (b)

From the Figure 4.14 (a), it is evident that the shape, width, and a combination of shape and width are the most important parameters in the reduction of the concentration values close to the obstacle. Shape of the obstacle plays an important role in the concentration reduction downwind; this behavior is different from the pool case, where the shape of the obstacle doesn't play an important role in the concentration reduction. The other important parameters are the height and width of the obstacle, similar compared with the pool case; however, with less contribution.

When the concentration is measured far away from the obstacle (at 82.5 m), besides the importance of the shape and width, a combined effect of both plays an important role in the concentration reduction, as shown in Figure 4.14 (b).

Table 4.5 summaries the effect list of the analyzed parameters and their contribution in the concentration reduction at 3 m and 82.5 m downwind the obstacle.

Table 4.5 Parameter contribution in concentration reduction for jet release case at distances: x = 3m and x = 82.5m

Parameter	**Contribution in concentration reduction (%)**	
	x= 3m	**x = 82.5m**
Shape	45.4	42.0
Width	34.5	20.6
Height	1.8	0.0
Wind Velocity	0.9	10.5
Shape&Width	11.7	13.7
Other parameters combination	11.2	13.2

Figure 4.15 and Figure 4.16 show the surface plots by interaction between the main parameters in the concentration reduction at a downwind distance x = 3m and x=82.5 m. Figure 4.15 (a) shows the efficiency in concentration reduction (in percentage) when either the wind velocity or the width of the obstacle are modified. By increasing the wind velocity, a concentration reduction of 90% can be obtained, while if the roughness is increased the concentration reduction is 82%. If both parameters are increased, the total reduction achieved is 92%. The same analysis could be done for Figure 4.15 (b) where an interaction between width and height of an obstacle is showed.

In the same way, Figure 4.16 shows the efficiency in concentration reduction by the interaction between other main parameters: wind velocity vs. height (a), and width vs. wind velocity (b); at a downwind distance x =82.5 m.

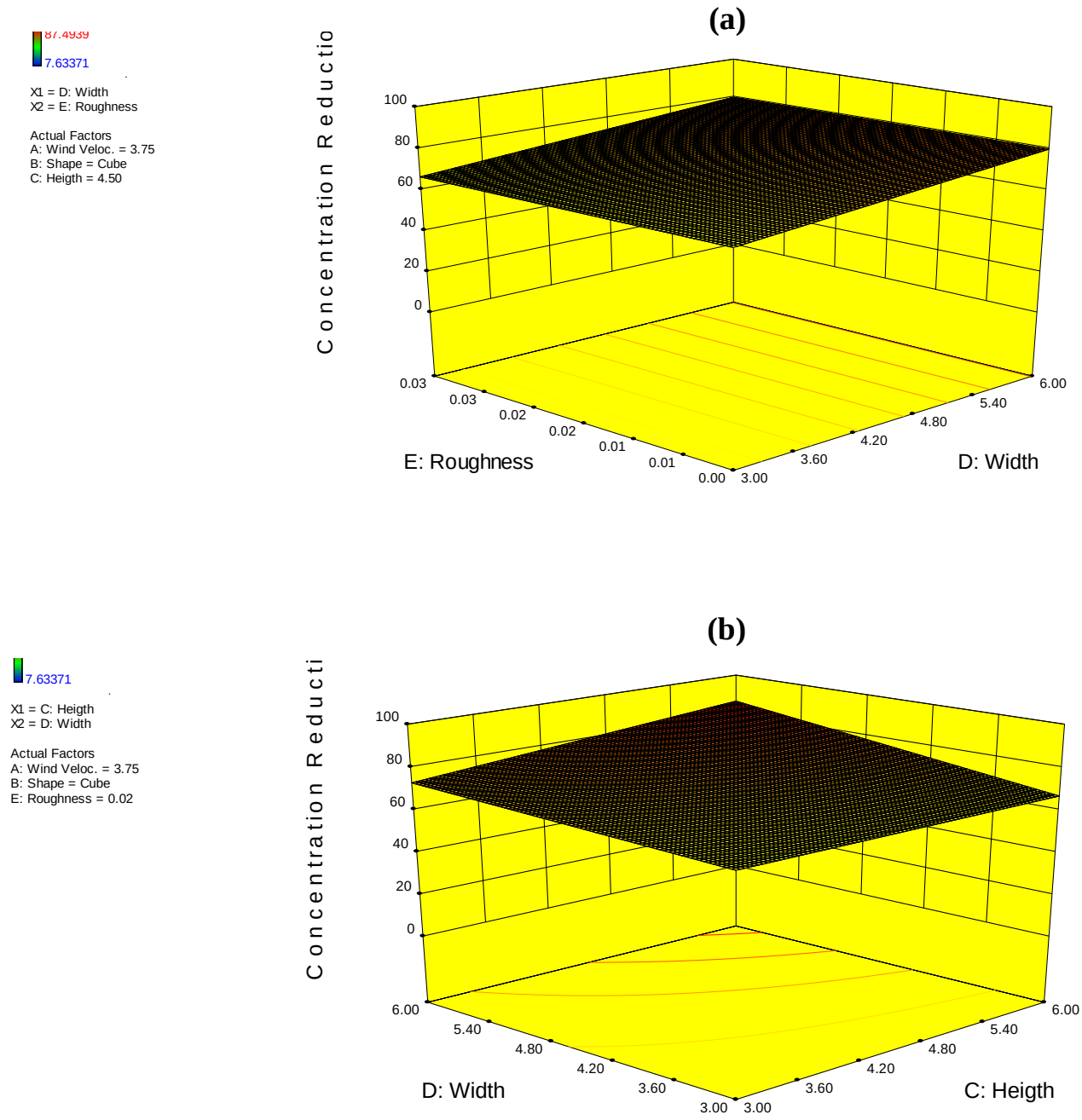

Fig. 4.15. Surface plots for parameter interaction at distance: x = 3 m

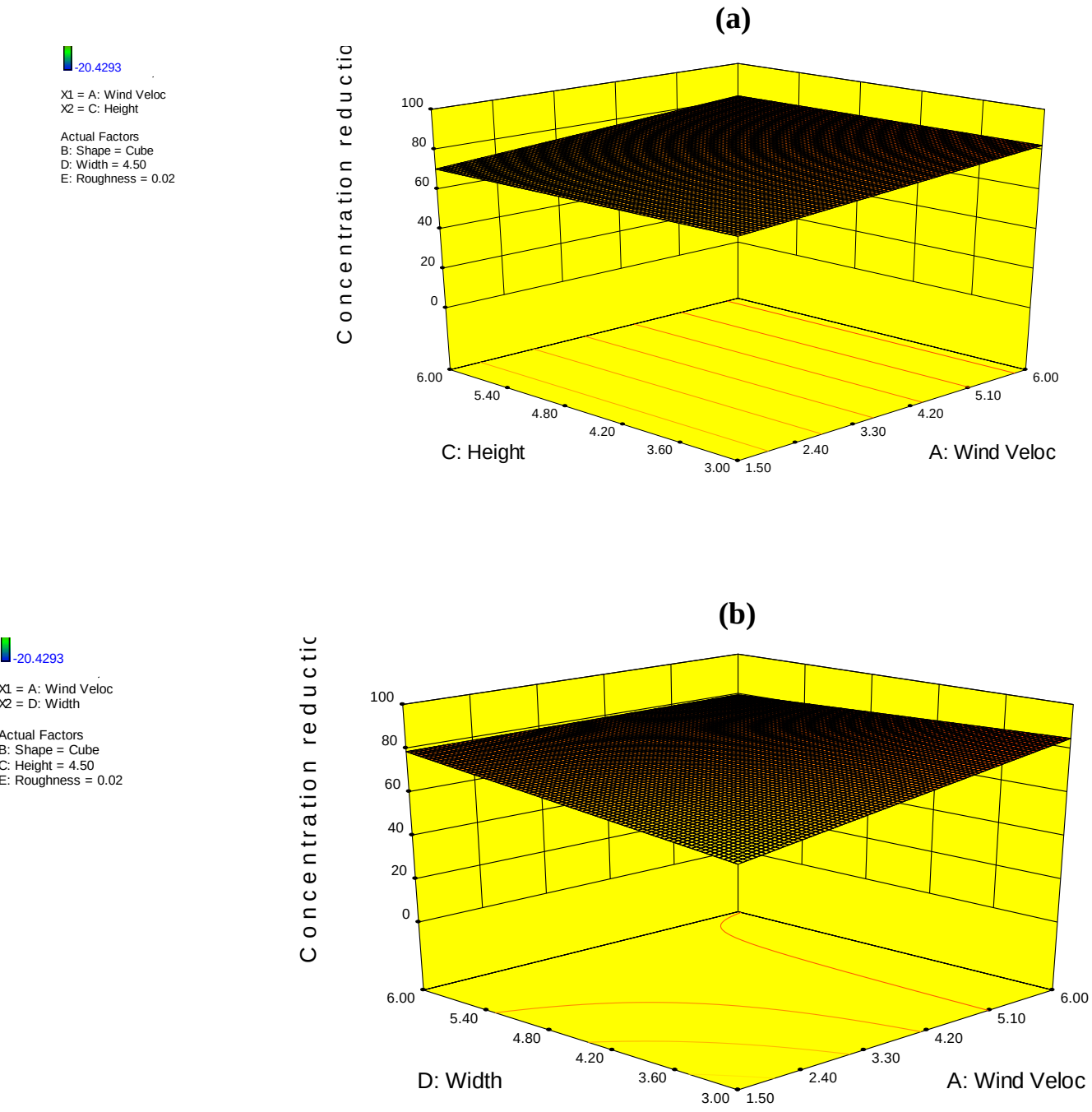

Fig. 4.16. Surface plots for parameter interaction at distance: x = 82.5 m

CHAPTER V

POTENTIAL APPLICATIONS

Parametric analysis demonstrates that the height and width of an obstacle have significant effect on LNG vapor dispersion. This chapter discusses the potential applications of this understanding. For example, optimization of the aspect ratio for LNG storage tank and separation distance (porosity) between them, that will help to reduce the LNG vapor concentration values and the safety distance.

Also specific cases will be studied; for instance, one of the conclusions of the parametric study was that the height, more than the width, plays a significant role in reducing downwind LNG vapor concentration. This understanding can be put into practice by designing a taller dike wall surrounding the LNG storage tank and decreasing the distance between the dike and tank wall so that the volume remains the same as suggested by the industry standard.

5.1 ANALYSIS OF ASPECT RATIO AND POROSITY

The previous parametric analysis focused on the effects that a single obstacle has over vapor dispersion and its impact in the concentration reduction. However, in an LNG facility a set of these obstacles are found and their effects will interact.

To address this issue, an analysis of the effects that LNG tanks have over vapor cloud is performed, considering a potential release of LNG in the storage area of a facility.

Aspect ratio of an obstacle is defined as the proportional relationship between its width and its height, as shown in equation 5.1:

$$Aspect\ ratio = \frac{Width\ of\ the\ obstacle}{Height\ of\ the\ obstacle} \tag{5.1}$$

On the other hand, porosity area is defined as the proportional relationship between the void-space and the total space of a determined surface. For this case study, they were considered tanks in a linear arrangement as indicated in Figure 5.1. The diameter of the tanks is represented by "d" and the distance between them is represented by "L".

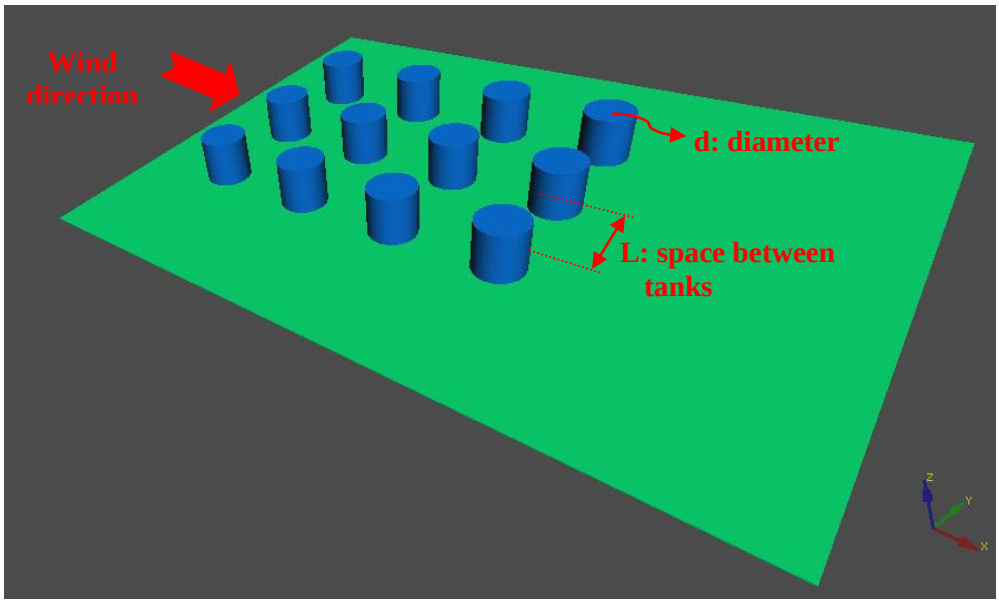

Fig. 5.1. Tanks' linear arrangement for aspect ratio and porosity analysis

Then, the porosity along the x axis is given by the equation 5.2:

$$Porosity\ (x) = \frac{2\,L}{3d + 2L} \tag{5.2}$$

The aspect ratio and porosity along the axis are related in this analysis, since an increase in the tank diameter produces a decrease in the porosity over the analyzed axis. The aspect ratios considered were 1, 1.5 and 2; while the porosity values obtained were 0.45, 0.38, and 0.34. How the aspect ratio of a tank influences in the concentration reduction of a vapor cloud has not been previously addressed; therefore, this analysis will provide new knowledge on this topic.

The release scenario simulated was an LNG leak due to a pipe rupture; the location of the leak was at x= 20 m, in front of the first tank of the storage area. Pool formation from the release was assumed, generating a vaporization rate of 110 kg/s for a total time of 10 minutes. The vapor generated will flow through the tanks from left to right, because the wind is assumed blowing in that direction with a velocity of 1.5 m/s. A roughness value of 0.03m was considered along the cloud path.

Figure 5.2 illustrates the flammability contours of the vapor cloud through three tank aspect ratios: 1, 1.5, and 2, at time t = 600 seconds. In Figure 5.2 can be seen the different behavior for the flammable contours of the vapor cloud when it passes through the tanks. It was observed that the distance traveled by the vapor cloud is slightly reduced when the porosity is reduced (diameter increase).

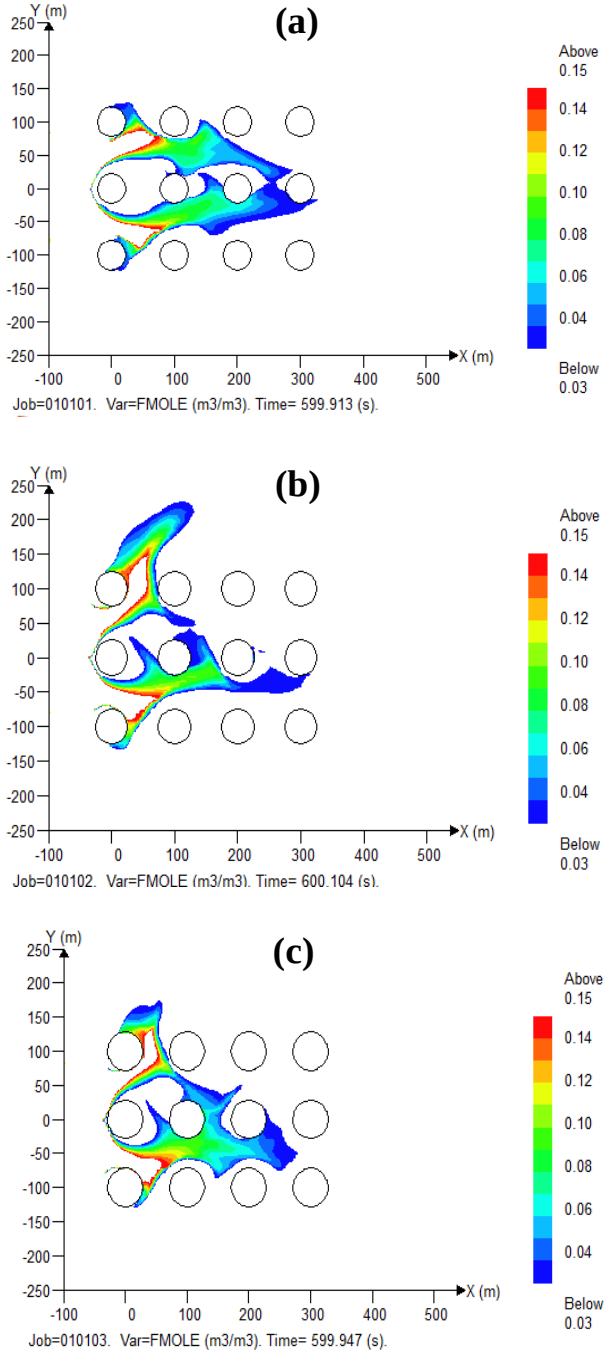

Fig. 5.2. Flammability contours through tanks with three different aspect ratios: (a) 1, (b) 1.5, and (c) 2.

A total of nine simulations were performed to combine the three different aspect ratios and porosities of the tanks. The vapor concentration values were taken at the end of the centerline of the storage area, and were compared in order to determine the vapor concentration reduction.

Figure 5.3 illustrates the concentration reductions (difference between concentrations with obstacles and without obstacles) obtained with the tanks at the analyzed aspect ratios and porosities along the x axis, measured at a distance of 50 m from the border line of the storage area.

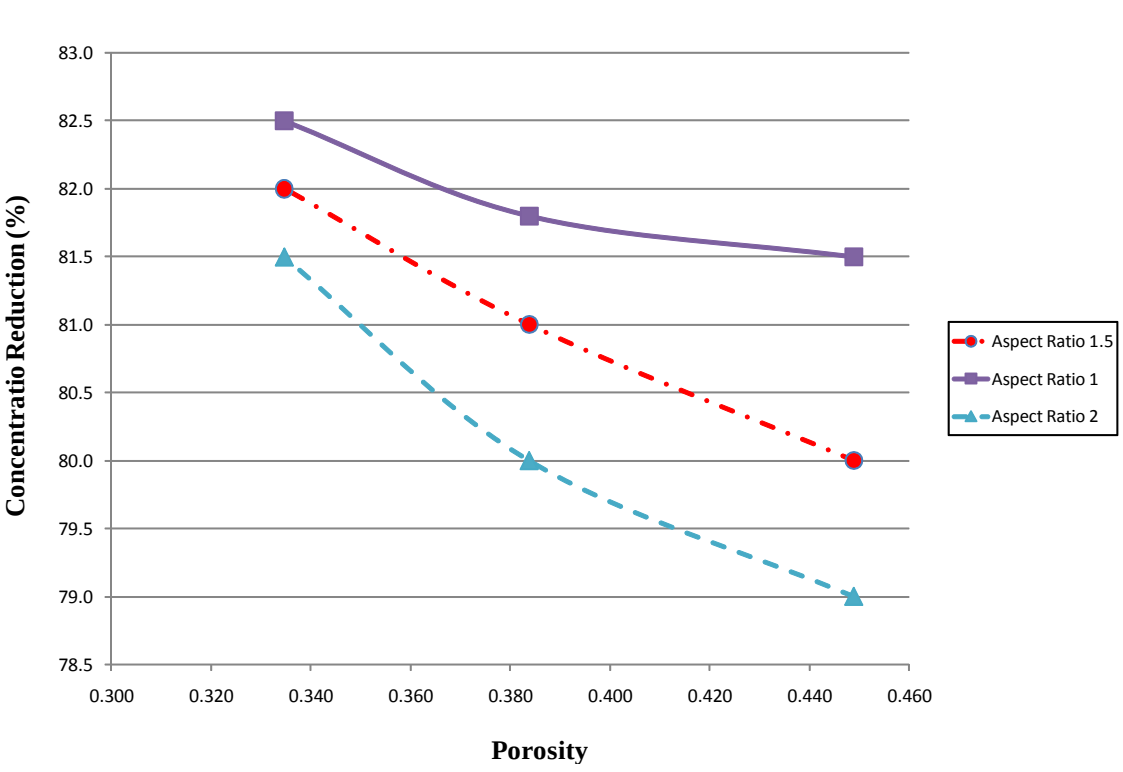

Fig. 5.3. Concentration reductions at different aspect ratios and porosities at 50 m from the storage area border line.

The importance of Figure 5.3 is that we can use it to estimate the vapor concentration reduction downwind from the LNG storage area by knowing the tanks' aspect ratio or the porosity, perpendicular to the wind direction. For instance, for a storage area containing tanks with an aspect ratio of 1.5 and a calculated porosity value of 0.34 (perpendicular to the wind direction), a concentration reduction of about 82% can be achieved. This improved understanding will help designers in making better decisions in regards to LNG facility layout and in determining the safety distances.

From Figure 5.3, it can be seen that the difference in the percentages between the concentration reductions achieved with the three aspect ratios is small, about 1.5 % between aspect ratio 1 and 1.5; and about 1.0 % between aspect ratio 1.5 and 2. Also, the results indicate that the concentration reduction is higher when the porosity along the "x" axis is diminished; in other words, when the diameter of the tanks is increased. The difference in reduction values between the highest and the lowest porosities analyzed is approximately 2.5%.

5.2 SPECIAL APPLICATIONS

5.2.1 Storage tanks' layout

Tanks' layout in an LNG facility is generally linear in arrangement of rows, similar to the arrangement showed in Fig 5.1. This case study analyzes a proposed new staggered configuration for the tanks within the storage area. The proposed new configuration of the tanks is intended to achieve lower concentration values downwind from the tanks, because of the diminishment in the porosity along the x axis created by this new tank arrangement. The wind was assumed to be blowing in the x direction from left to right at a velocity of 1.5 m/s, at neutral atmospheric stability conditions. A typical roughness of 0.03m was considered along the cloud path.

A scenario of a pipe rupture and LNG leak is assumed to begin at a location x= 20 m at the beginning of the tank storage area. The release time is 10 minutes and pool formation is assumed, with a vaporization rate of 110 kg/s. The vapor cloud generated will pass through the tanks from left to right and measurements of the vapor concentration are taken at the end of the storage area, along the centerline.

Figure 5.4 shows the flammable vapor cloud (5-15% in concentration volume) at a time t= 650 seconds, for a set of tanks with three different aspect ratios: 1, 1.5, and 2.

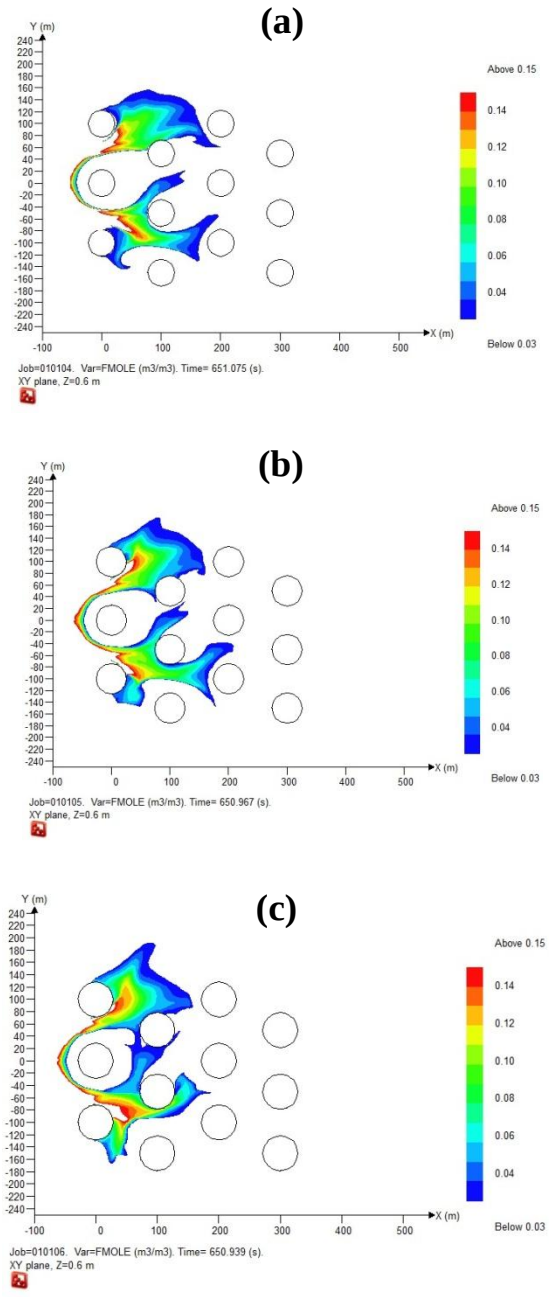

Fig. 5.4. Flammability contours through tanks with three different aspect ratios (staggered layout): (a) 1, (b) 1.5, and (c) 2.

Figure 5.4 illustrated the different behavior for the vapor cloud passing through the tanks. It is observed that the cloud surrounds the tanks more closely when the diameter (and aspect ratio) is increased and the cloud travels a lower downwind distance. Therefore, in this case the variation of the aspect ratio as well as the different layout of the tanks plays an important role.

A comparison between the reductions in the concentration values obtained with the two different tank layouts is performed. Both cases have the same scenario assumptions and set up. Figure 5.5 shows the vapor cloud behavior for these cases with an aspect ratio of 2, at a time of 750 seconds.

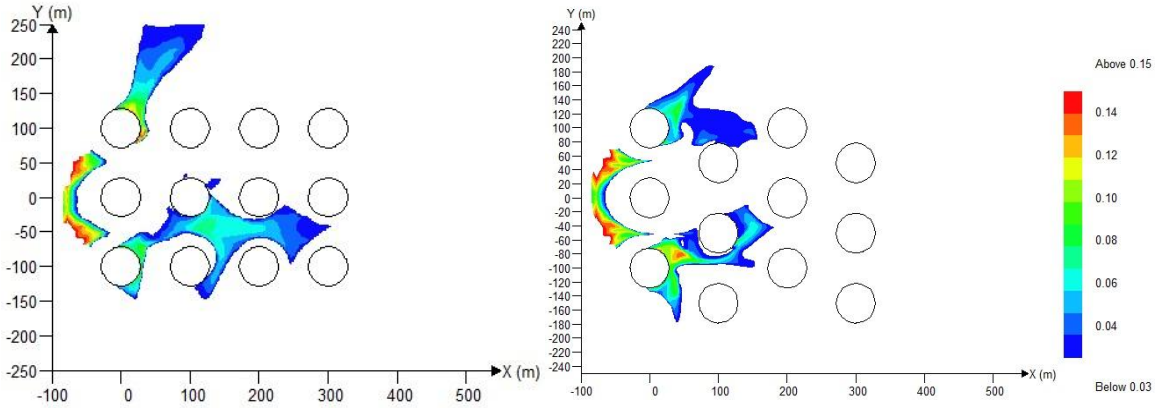

Fig. 5.5. Comparison of flammability contours at different tanks' layout, with aspect ratio = 2, at t = 750 s.

This study concludes that reduction in the concentration values downwind from the storage area is possible by changing the tanks' layout, and therefore a reduction in the safety distance can be achieved as well. Table 5.1 summarizes the concentration reduction percentages in the analyzed cases, for a measurement point located at a distance x = 200m from the borderline of the storage area.

Table 5.1 Concentration reduction percentage at different tanks' layout

	Concentration Reduction (%)		Conc. Reduction Difference (%)
	Linear layout	Staggered layout	
Aspect Ratio 1 - Porosity1	81.5	92.3	**10.83**
Aspect Ratio 2 - Porosity 2	81.5	92.7	**11.16**
Aspect Ratio 3 - Porosity 3	81.5	96.6	**15.05**

5.2.2 Dike design

According to the parametric analysis performed in Chapter IV, an increase in the height of an obstacle plays an important role in reducing the vapor concentration values. NFPA 59A indicates that an impoundment system (dike) must be designed to contain a possible LNG spill equal to the 110% of the largest tank associated with that system. This case study will analyze the importance of a good design of an LNG dike in

reducing the safety distance, by varying its height and width, while maintaining the same volume. A typical LNG tank with a capacity of 50,000 m^3 was considered, and the dimensions of the dike surrounding it were 110m x 110m x 5m, which comply with NFPA 59A requirements in volume capacity.

For the purpose of this case study, modification in the dimensions of the dike was done by increasing its height from 5m to 8m, but diminishing its sides from 110m to 85m. Figure 5.6 shows the two different analyzed dikes (dike 1 and dike 2).

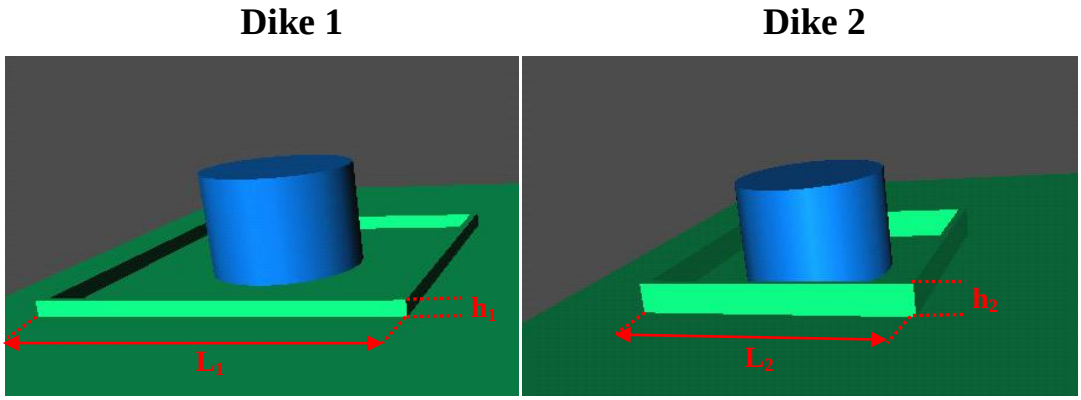

Fig. 5.6. Comparison between two different dike designs; dike1: 110 x 110 x 5 m, dike2: 85 x 85 x 8 m.

The largest accidental release scenario was considered by a leakage caused by the rupture of a pump-out transfer piping located within the dike area, with a flow rate of 2000 m^3/h when all the pumps are running.

According to the NFPA 59A requirements, the impoundment system has to withstand that spill during 10 minutes. An F stable atmospheric condition with a wind speed of 1.5 m/s was considered as the worst case scenario, and a roughness value of z_0 = 0.03 m was considered as well.

Regarding the simulation details, the meshing was carefully performed and refined close to the LNG spill, the tank, and dike. The control volumes' dimensions were 0.8m in the x and y directions, and 0.5m in the z direction. The measurement points for gas concentration were located along the centerline, downwind of the dike borderline at distances of 50m and 200m. The FLACS pool model was used to simulate the pool formation inside the dike. Figure 5.7 shows the simulation results of the pool generated within Dike2 using FLACS at a time t = 600 seconds.

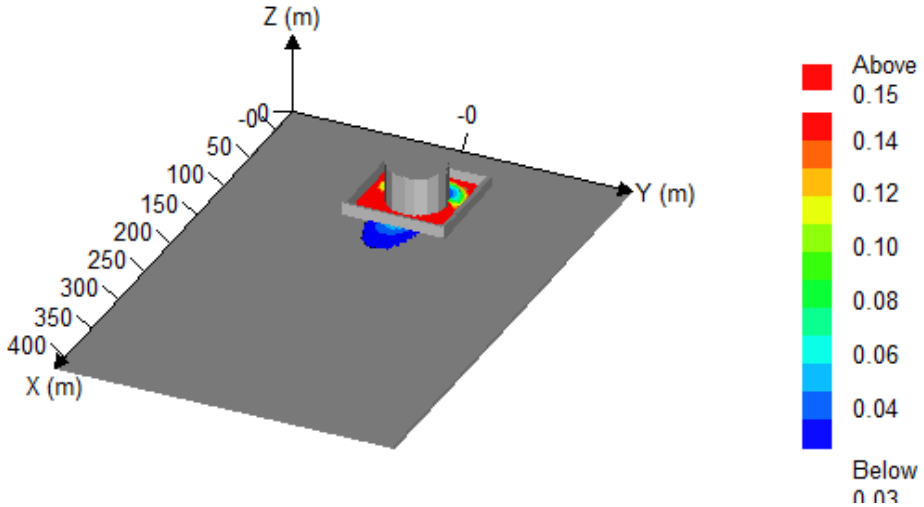

Fig. 5.7. Pool formation within dike 2 at time 600 seconds

The same conditions of the explained scenario were used in the second type of dike, maintaining the location of the leakage considered previously. The results obtained indicate that by increasing the height of a dike, the vapor concentration is reduced and therefore the safety distance, defined as the distance where the half of the LFL is obtained. Figure 5.8 shows the comparison between the safety distances obtained with the two different dikes.

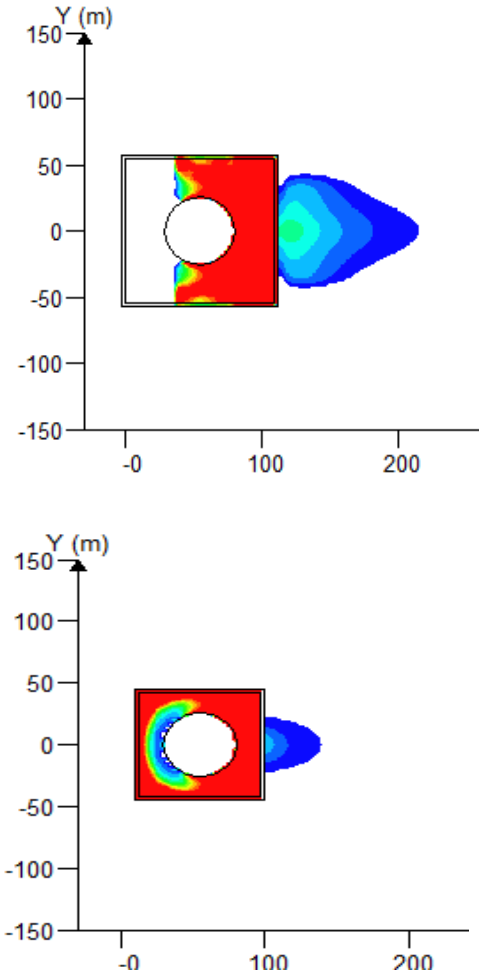

Fig. 5.8. Comparison between safety distances with the two different analyzed dikes

It is important to note that constructing a dike involves money and time investment; therefore, a cost/benefit assessment needs to be done in order to make the decision if a dike with higher walls is necessary. The second type of dike (with higher walls) provides advantages in terms of space within the facility. Also, risk reduction is achieved because the flammable LNG vapor will travel a lower distance. Figure 5.9 shows the comparison between the safety distances obtained with both type of dikes; for Dike1 the distance obtained was 220 m, while for Dike 2 it was 140 m. The results also indicate a reduction in about 35% for the safety distance based on the ½ LFL standard.

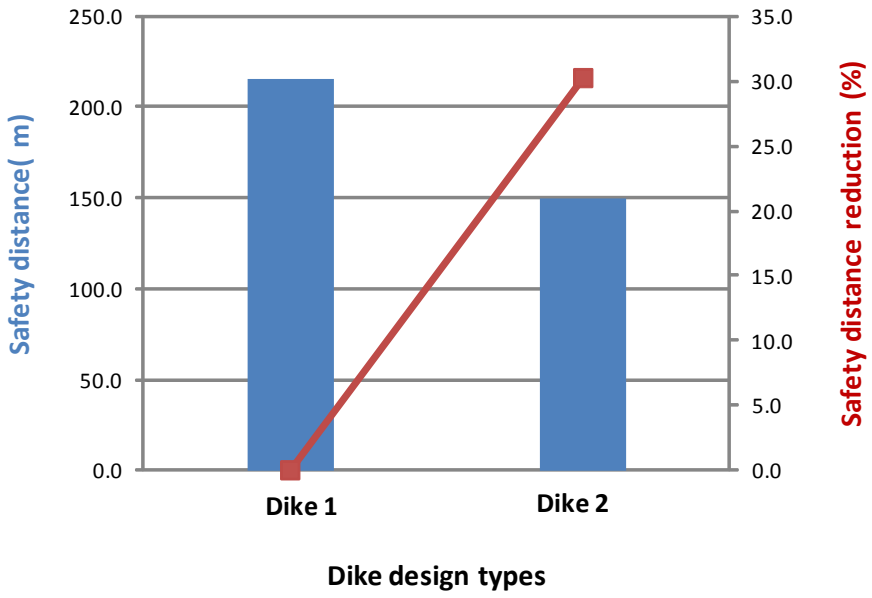

Fig. 5.9. Safety distance reduction with two different dike dimensions

CHAPTER VI

CONCLUSIONS AND FUTURE WORK

6.1 CONCLUSIONS

This research demonstrated that the effect of obstacles over LNG vapor dispersion plays an important role in reducing downwind concentration values and achieving lower safety distances. This knowledge may be applied in facility layout of an LNG terminal and also in the design of an LNG impoundment dike.

This research provides several contributions as follows:

- Establish a CFD model suitable to simulate LNG vapor dispersion through obstacles, similar to those found in an LNG facility.
- Validation of developed model. The result obtained by the FLACS model in this work was compared with the Falcon experimental data and with previous simulation result obtained by FLUENT model. It was demonstrated that FLACS model indeed provides a reasonably accurate simulation of LNG source and vapor dispersion.
- Perform a parametric analysis over the selected key parameters involved in vapor dispersion through obstacles: height, width, and shape of the obstacle as well as wind velocity and surface roughness, for cases of LNG pool release and jet release. For the pool release case, the results of the analysis demonstrated that height and width of an obstacle are the most significant parameters in the LNG vapor concentration reduction, for values measured close to the obstacle. If the

measurement is done far away from the obstacles, a combination of the wind velocity and surface roughness also becomes more important. For the jet release case, shape and width of the obstacle are the two most significant parameters in LNG vapor concentration reduction, for values measured either near or far from the obstacle.

- Propose a methodology which may be used in an LNG facility to estimate the LNG vapor concentration reduction downwind from the storage area. Using Figure 5.3, one can estimate the concentration reduction by knowing either the tanks' aspect ratio or the porosity perpendicular to the wind direction. This methodology could help to assess safety distances during the design stage of an LNG facility.
- Based on the research finding two possible design improvements were suggested for reducing downwind LNG vapor concentration and safety distance.

  They are staggered configuration for the LNG storage tanks and increased height of the impoundment dike wall. It was demonstrated that staggered layout provides an improvement of about 15% in the concentration reduction compared to the usual linear layout. In the case of the new dike design, the reduction of the safety distance was about 35% (reduced from 220 m to 140 m) providing advantages in terms of space within the facility as well as in risk reduction.

6.2 FUTURE WORK

This research increased the knowledge acquired so far by MKOPSC about the effects of obstacles in vapor dispersion; however, there are some potential possibilities to further explore this topic; they are:

- Study the effects of turbulence inside a storage area for different LNG tank configurations. This research focused on the effects of obstacles over the vapor concentration reduction; however, it is promising to study the increase in turbulence generated by tank configurations.
- The increment in turbulence by tank configurations, similar to the proposed staggered layout, may create an explosion hazard inside the storage area. An analysis using a CFD tool may be useful to assess this scenario.
- Possible small or medium scale experiments which account for the effects of different obstacles on LNG vapor dispersion can be performed. In this manner, the proposed tank configurations and dike design could be studied and the results of this research validated.
- Evaluate new possible dike designs which intend to reduce the vapor concentration and the safety distance. This research demonstrated the importance of height in dikes; however, this design can be improved in future by adding a overhang portion on the top of the dike. This may cause recirculation of the vapor, retaining it for more time and promoting turbulence and mixing with air.

REFERENCES

Bosch, C., & Weterings, R. (2005). *Methods for the calculation of physical effects due to releases of hazardous materials (liquids and gases) 'Yellow Book'* (3rd ed.). The Hague: Gevaarlijke Stoffen.

Brown, T., Cederwall, T., Chan, S., Ermak, D., Koopman, R., Lamson, K., McClure, J., & Morris, L. (1990). Falcon series data report: 1987 LNG vapor barrier verification field, Gas Research Institute. *Report No. GRI-89/0138.*

Chan, S.T. (1992). Numerical simulations of LNG vapor dispersion from a fenced storage area. *Journal of Hazardous Materials*, *30*, 195-224.

Chan, S.T. (1994). FEM3C: *An improved three-dimensional heavy-gas dispersion model: user's manual.* California: Lawrence Livermore National Laboratory.

Coldrick, S., Lea, C., & Ivings, M. (2010). *Validation Database for Evaluating Vapor Dispersion Models for Safety Analysis of LNG Facilities - Guide to the LNG Model Validation Database*. Massachusetts: The Fire Protection Research Foundation.

Conrado, C., & Vesovic, V. (2000). The influence of chemical composition on vaporization of LNG and LPG on unconfined water surfaces. *Chemical Engineering Science, 5*, 4549–4562.

Cormier, B. (2008). *Computational fluid dynamics for LNG vapor dispersion modeling: A key parameter study.* PhD dissertation, Texas A&M University. College Station, Texas.

Cormier, B., Suardin, J., Rana, M., & Zhang, Y. (2009). Development of design and safety specifications for LNG facilities based on experimental and theoretical research, in: E.R. Pitt, C.N. Leung (Eds.). *Nova Science Publishers*, 2009.

Crowl, D.A., & Louvar, J.F. (2002). *Chemical Process Safety Fundamentals with Applications* (2nd Ed). New Jersey: Prentice Hall PTR.

DeLoach, R., & Ulbrich, N. (2008). A Comparison of Two Balance Calibration Model Building Methods. *Report by American Institute of Aeronautics and Astronautics*. Virginia: NASA.

EIA (Energy Information Administration). (2009). Energy in brief - What everyone should know about energy. http://www.eia.gov. Last accessed 06.14.12.

Gavelli, F., Bullister, E., & Kytomaa, H. (2008). Application of CFD (Fluent) to LNG spills into geometrically complex environments. *Journal of Hazardous Materials*, *159*, 158-168.

Gexcon AS. (2011). *FLACS v9.1 User's Manual*. Norway: GexCon AS.

Gexcon website. (2012). FLACS software information. http://www.gexcon.com/. Last accessed 06.14.12.

Golder, D. (1972). Relations among stability parameters in the surface layer. *Boundary-Layer Meteorology*, *3*, 47–58.

Han, J., Arya, S.P., Shaohua Shen, & Yuh-Lang. (2000). *An Estimation of Turbulent Kinetic Energy and Energy Dissipation rate Based on Atmospheric Boundary Layer Similarity Theory*. North Carolina: NASA.

Hankin, R. (2003). Heavy gas dispersion: Integral models and shallow layer models. *Journal of Hazardous Materials*, *102*, 1–10.

Hanna, S., Hansen, O., & Dharmavaram, S., (2004). FLACS CFD air quality model performance evaluation with Kit Fox, MUST, Prairie Grass, and EMU observations. *Atmospheric Environment*, *38*, 4675-4687.

Hansen, O., Melheim, J. & Storvik, I. (2008). *Validating the data, LNG Industry – a supplement to Hydrocarbon Engineering.* Spring Issue.

Hansen, O., Gavelli, F., Ichard, M & Davis, S. (2010). Validation of FLACS against experimental data sets from the model evaluation database for LNG vapor dispersion. *Journal of Loss Prevention in the Process Industries*, *23*, 857-877.

MacDonald, R., Griffiths, R. & Hall, D. (1998). An improved method for the estimation of surface roughness of obstacles arrays. *Atmospheric Environment, 11*, 1857-1864.

Martinuzzi, R., & Tropea, C. (1993). The Flow Around Surface-Mounted, Prismatic Obstacles Placed in a Fully Developed Channel Flow (Data Bank Contribution). *Journal of Fluids Engineering*, *1*, 85-93.

Mavroidis, I., Griffiths, & R., Hall, D. (2003). Field and wind tunnel investigations of plume dispersion around single surface obstacles. *Atmospheric Environment*, *37*, 2903-2918.

MKOPSC (Mary Kay O'Connor Process Safety Center). (2008). *White Paper: LNG Pool Fire Modeling, M.S. Mannan (Editor)*. Texas A&M University. College Station, Texas.

MKOPSC (Mary Kay O'Connor Process Safety Center). (2010). *Data report of MKOPSC LNG spill tests: 2005-2009.* Texas A & M University, College Station, Texas.

Monin, A. S., & Obukhov, A. M. (1954). Basic laws of turbulent mixing in the surface layer of the atmosphere. *Tr. Akad. Nauk SSSR Geofiz. Inst. 24*, 163-187.

Montgomery, D., & Runger, G. (2006). *Applied Statistics and Probability for Engineers* (5th Ed.). New Jersey: John Wiley & Sons, Inc.

NFPA (National Fire Protection Agency). (2009). *Standard for the production, storage, and handling of liquefied natural gas (LNG)*. NFPA 59 A: Edition 2009.

Ogawa, Y., & Oikawa, S. (1982). A field investigation of the flow and diffusion around a model cube. *Atmospheric Environment, 16*, 207 – 222.

Petersen, R. (1990). Effect of homogeneous and heterogeneous surface roughness on heavier-than-air gas dispersion. *Journal of wind engineering and industrial aerodynamics*, *36*, 643-652.

Puttock, J. (1987). *Comparison of Thorney Island data with predictions of HEGABOX/HEGADAS*. *Journal of Hazardous Materials*, *16*, 439-455.

Qi, R. (2011). *Liquefied Natural Gas (LNG) Vapor Dispersion Modeling with Computational Fluid Dynamics Codes.* PhD dissertation, Texas A&M University. College Station, Texas.

Qiao, Y., West, H., Mannan, M., Johnson, D., & Cornwell, J. (2006). Assessment of the Effects of Release Variables on the Consequences of LNG Spillage onto Water using FERC models. *Journal of Hazardous Materials*, *130*, 155-162.

Raj, P. (2005). Large LNG Fire Thermal Radiation – Modeling Issues & Hazard Criteria Revisited. *Process Safety Progress*, *3*, 192-202.

Raj, P. (2007). *LNG fires:* A review of experimental results, models and hazard prediction challenges. *Journal of Hazardous Materials*, *140*, Issue 3.

Robins, A., Castro, I. (1977). A wind tunnel investigation of plume dispersion in the vicinity of a surface mounted cube – I. The flow field. *Atmospheric Environment, 11*, 291 – 297.

Spicer, T.O., & Havens, J.A. (1987). Field test validation of the Degadis model. *Journal of Hazardous Materials*. *16*, 231-245.

U.S. Department of Transportation. (2002). *Liquefied Natural Gas Facilities: Federal Safety Standards.* Code of Federal Regulations: 49 CFR 193, Part 193. New York: USDOT.

VITA

Roberto Eduardo Ruiz Vásquez received his Bachelor of Science degree in electro-mechanical engineering from Pedro Ruiz Gallo University at Lambayeque – Peru in 2001. He started the Master of Science in Safety Engineering at Texas A&M University in January 2010 and received his Master of Science degree in August 2012. His research interests include consequence modeling and LNG vapor dispersion modeling.

Mr. Ruiz may be reached at 3122 TAMU College Station, TX 77843. His email address is ponciano@neo.tamu.edu.